PL-TR-95-2081

MODE CONVERSION IN AN OXYGEN-HYDROGEN PLASMA

Jay R. Johnson
Tom Chang
G. B. Crew

Massachusetts Institute of Technology
Center for Space Research
Cambridge, MA 02139

22 March 1995

Scientific Report No.3

PHILLIPS LABORATORY
Directorate of Geophysics
AIR FORCE MATERIEL COMMAND
HANSCOM AIR FORCE BASE, MA 01731-3010

"This technical report has been reviewed and is approved for publication"

(Signature)
BAMANDAS BASU
Contract Manager

(Signature)
DAVID N. ANDERSON
Branch Chief

(Signature)
WILLIAM K. VICKERY
Division Director

This report has been reviewed by the ESC Public Affairs Office (PA) and is releasable to the National Technical Information Service (NTIS).

Qualified requestors may obtain additional copies from the Defense Technical Information Center (DTIC). All others should apply to the National Technical Information Service (NTIS).

If your address has changed, if you wish to be removed from the mailing list, or if the addressee is no longer employed by your organization, please notify PL/IM, 29 Randolph Road, Hanscom AFB, MA 01731-3010. This will assist us in maintaining a current mailing list.

Do not return copies of this report unless contractual obligations or notices on a specific document requires that it be returned.

REPORT DOCUMENTATION PAGE

Form Approved
OMB No. 0704-0188

1. AGENCY USE ONLY (Leave blank)	2. REPORT DATE	3. REPORT TYPE AND DATES COVERED
	22 March 1995	Scientific No. 3

4. TITLE AND SUBTITLE

Mode Conversion in an Oxygen-Hydrogen Plasma

5. FUNDING NUMBERS

PE 61102F
PR 2310 TA G6 WU EA

Contract F19628-91-K-0043

6. AUTHOR(S)

Jay R. Johnson, Tom Chang and G. B. Crew

7. PERFORMING ORGANIZATION NAME(S) AND ADDRESS(ES)

Massachusetts Institute of Technology
Center for Space Research
Cambridge MA 02139

8. PERFORMING ORGANIZATION REPORT NUMBER

9. SPONSORING / MONITORING AGENCY NAME(S) AND ADDRESS(ES)

Phillips Laboratory
29 Randolph Road
Hanscom Air Force Base, MA 01731-3010
Contract Manager: Bamandas Basu/GPIM

10. SPONSORING / MONITORING AGENCY REPORT NUMBER

PL-TR-95-2081

11. SUPPLEMENTARY NOTES

12a. DISTRIBUTION / AVAILABILITY STATEMENT

approved for public release:
distribution unlimited

12b. DISTRIBUTION CODE

13. ABSTRACT *(Maximum 200 words)*

The complications of mode-conversion which occur near a minority resonance are studied in the context of electromagnetic ion-cyclotron heating of a minority oxygen population in the magnetosphere. This problem is investigated using several different approaches. A perturbation approach demonstrates that the coupling results from non-parallel propagation. The phase-integral approach involves analytic continuation of (WKB) solutions and involves a discontinuity in the Poynting flux corresponding to energy absorption. The saddle point approach emphasizes the degree to which the coupling can be analyzed in terms of two mode coupling processes. When the two low frequency propagating modes coalesce near the oxygen resonance at two different coupling points, a numerical scheme which retains the two coupling points in a realistic manner is employed, and numerical coefficients are obtained. The calculated coefficients that are presented demonstrate that substantial coupling occurs between the two propagating modes and a definite absorption occurs. Such absorption is sufficient to explain the outflow and heating of ionospheric oxygen ions.

14. SUBJECT TERMS

mode conversion, ion cyclotron waves, WKB approximation, oxygen-hydrogen plasma, ion heating

15. NUMBER OF PAGES

74

16. PRICE CODE

17. SECURITY CLASSIFICATION OF REPORT	18. SECURITY CLASSIFICATION OF THIS PAGE	19. SECURITY CLASSIFICATION OF ABSTRACT	20. LIMITATION OF ABSTRACT
unclassified	unclassified	unclassified	SAR

Contents

List of Figures

Part 1
An Analytical Study of Mode Conversion

1 Introduction

It is well known that wave propagation in a multiple species plasma is substantially modified near the ion resonances[*Buchsbaum*, 1960a, 1960b]. This modification leads to important effects which can be utilized, for example, as a diagnostic to determine plasma concentration[*Gurnett et al.*, 1965] or as a tool to heat plasma via ion-cyclotron resonance heating (ICRH)[*Swanson*, 1976; *Jacquinot et al.*, 1977; *Perkins*, 1977]. The effects of a minority plasma are substantial in that modes which would not ordinarily heat cold ions may energize the minority population. In this report, we address wave propagation in a multispecies plasma in the context of a specific problem of importance in space physics. In this problem, waves propagate from a region of small magnetic field into a region of increasing magnetic field. In some localized region the waves encounter the local minority ion gyrofrequency (oxygen in this case) and wave power is reflected, transmitted, mode converted, and absorbed. Under reasonable conditions, the wave power absorbed by the minority species is sufficient to energize ions to observed energies.

One of the more intriguing phenomena of space physics is the energization of ionospheric plasma to magnetospheric energies. A particular manifestation of this outflow are the events termed ion conics. Ion conics are essentially the signature of a heating process transverse to the magnetic field. The conic shape (distribution with a fixed pitch angle in velocity space) may be heuristically understood in terms of conservation of the first adiabatic invariant where perpendicular energy is converted into parallel energy in the geometry of a decreasing magnetic field.

One particular variety of conic which has provided remarkable confirmation of theory is that which is observed along closed field lines which emanate from the auroral region into the central plasma sheet (CPS). These conics are generally observed in association with a broadband spectrum of downcoming waves which peaks at low frequencies and contains substantial

wave energies at the local oxygen cyclotron frequency [*Gurnett et al.*, 1984]. *Chang et al.* [1986] suggested a heuristic model in which these waves interact resonantly with ions over an extended altitude corresponding to a range of cyclotron resonance with the broad range of frequencies within the observed spectrum. The energies and pitch angles of the conics were in agreement with this model. Moreover, a more rigorous analysis [*Retterer et al.*, 1987; *Crew and Chang*, 1988; *Crew et al.*, 1990] not only confirmed this theory, but provided what may be the best agreement between theory and observation in space physics. Perhaps the most remarkable aspect of this analysis is that it contained only one free parameter, namely the fraction of left-hand circular polarization (LHCP) (i.e. the amount of wave power which can resonate with the ions). Although the mechanism by which the conics are formed seems to be well understood, the origin and nature of the ambient turbulence remain somewhat uncertain.

The existence of these waves has remained somewhat of a mystery in that careful scrutiny of the data has to date precluded a local source (very little free energy is available in this region of the magnetosphere). In light of the observations associated with the conic events, we suggested a scenario [*Johnson et al.*, 1989] in which the waves are generated in the equatorial region of the magnetosphere, propagate along magnetic fields to lower altitudes (larger magnetic field) and are then absorbed, to some extent, at the local cyclotron resonance. In this manner, the minority oxygen is energized to magnetospheric energies. According to this scenario as well as direct satellite measurement of the Poynting flux, the source of the observed spectrum would appear to be from "above" the region in which ion-heating occurs. That is, the waves propagate from regions of small magnetic field into regions of large magnetic field. An obvious question then arises. How much of the wave energy is absorbed by ions at the local oxygen resonance, and is that absorption sufficient to energize the ions to magnetospheric energies?

The purpose of this present work is, therefore, to demonstrate that the assumed absorption of wave energy by the ion conics is appreciable within the framework of a reasonable model. In order to determine the amount of wave absorption, we simplify the geometry and make suitable approximations which retain the most essential gradients involved in the wave equations. It will be obvious from the structure of these equations that the four low frequency cold plasma modes couple strongly near the minority ion gyrofrequency. Hence, power may be exchanged between the modes so that both the

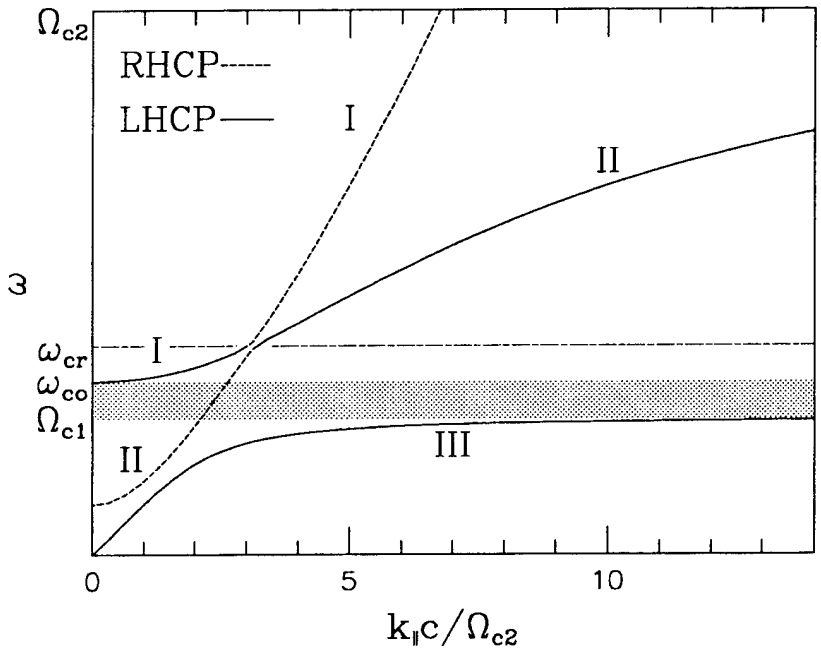

Figure 1: Dispersion relation for a cold two ion component plasma for nonparallel propagation. The various branches are labeled according to their predominate polarization with RHCP dashed and LHCP solid. Coupling occurs at the crossover frequency (ω_{cr}) where the polarization of branches I and II switches abruptly. Tunneling occurs across the shaded "gap" between the cutoff frequency (ω_{co}) and the heavy ion gyrofrequency (Ω_{c1}).

magnetosonic and shear Alfvén modes can undergo substantial absorption. We analyze these mode conversion problems using a variety of techniques. We obtain analytical results using a perturbation analysis, the saddle-point method, and the phase-integral method, and we discuss parallel work which employs an asymptotic expansion of the Fourier transform of the differential equation. The various approaches each provide some insight as to the physics described by the equations. In part 2 of this report we present a numerical solution which provides not only a check of the analytical results, but also serves to retain the presence of multiple saddle points which are, in some cases, not well approximated by an analytical solution.

In order to understand more completely the processes which we are examining, consider the dispersion relation of Figure 1. This dispersion relation is characterized by three separate modes which we have labeled I, II, and

III. Mode I is the magnetosonic branch and is predominately right-hand circularly polarized at high frequency whereas mode II, which is the hydrogen ion-cyclotron branch, is predominately LHCP. Below the oxygen cyclotron frequency mode II continues to propagate as the right-hand circularly polarized (RHCP) magnetosonic branch and mode III represents the LHCP ion-cyclotron branch. Near the crossover frequency (the relevant frequencies in a multispecies plasma are discussed in Appendix C), modes I and II couple and exchange energy [*Smith and Brice*, 1964]. Mode I also suffers a cutoff at the cutoff frequency and is separated from mode III by an evanescent region. As waves move into regions of larger magnetic field they move "down" along the dispersion curves according to the WKB approximation in that they satisfy the local dispersion relation. The scenario in which waves propagate earthward into a region of larger magnetic field (as is the case for waves propagating from the equatorial region to the auroral region) corresponds to waves incident from "above" the coupling-evanescent region. Some of the incident wave power is then reflected back along branches I and II, some wave power is transmitted along branches II and III "below" the heavy ion cyclotron frequency, and some wave power is absorbed in the evanescent region. Particle heating may result from ion-cyclotron damping of branch III (for a thermal plasma) and from the calculated absorption which typically corresponds to mode conversion to a thermal plasma wave which is strongly damped.

2 Basic Equations

Our goal is to describe the behavior of low frequency waves near the series of crossover cutoff and resonance frequencies found in a multispecies plasma. In the CPS the typical Alfvén wavelength far exceeds even the most energetic ion gyroradius so that a cold plasma description is reasonable. The essential feature that we wish to retain is the variation of the magnetic field strength along field lines (density gradients do not affect the location of the resonances and only density ratios affect the location of the other special frequencies). The differential equations are most tractable and still retain the essential features which we wish to incorporate into our analysis if we consider a plasma in which the mode conversion processes are dominated by the variation in the strength of the magnetic field along one dimension and

take the density to be constant.

At low altitudes where the heating and mode conversion processes are presumed to occur, the primary variation in the magnetic field strength is along the direction of the magnetic field. Thus, we assume that the only magnetic field variations are along the field line, and we neglect the variations perpendicular to the field line and, in effect, the field line curvature. Such an approximation is reasonable if the conversion process is localized in some sense with respect to the scale length of the magnetic field. Indeed, the scale over which the mode conversion occurs is asymptotically small compared with variations in the magnetic field so that such an approximation is valid.

We should emphasize that perpendicular gradients are weak compared to parallel gradients for this problem so that their effects are not important in our calculations. Thus, our work is different from other studies in which perpendicular gradients dominate [*Swanson*, 1976; *Jacquinot et al.*, 1977; *Perkins*, 1977]. We should point out that variations perpendicular to the magnetic field do not couple the two propagating cold plasma modes in that wave propagation across the field is described by a second order differential equation. However, it should be noted that variations across the field should give rise to coupling between cold plasma waves and thermal ion-ion harmonic waves [*Swanson*, 1976; *Jacquinot et al.*, 1977; *Perkins*, 1977].

Maxwell's equations combined with the momentum transfer equations describe wave propagation in a plasma medium [*Stix*, 1962]. In light of the approximations detailed above, these equations reduce to a set of coupled ordinary differential equations for the components of the electric field [*Försterling*, 1942]. For low frequencies, the electric field parallel to the magnetic field becomes negligible [*Swanson*, 1989] so that the equations for the circularly polarized electric field components perpendicular to the magnetic field, $E_\pm = E_x \pm iE_y$ take the compact form

$$\epsilon^2 \Psi'' + \mathbf{M}\Psi = 0 \tag{1.1}$$

where

$$\mathbf{M} = \begin{pmatrix} r - \kappa^2/2 & \kappa^2/2 \\ \kappa^2/2 & l - \kappa^2/2 \end{pmatrix} \tag{1.2}$$

The vector Ψ consists of two components E_- and E_+ which we will also refer to as ψ and ϕ. The characteristics of the medium are contained in the parameters: $\epsilon = 1/k_A L_B$, $\kappa = k_\perp/k_A$, $k_A = \omega/v_A$, $L_B = B^{-1}dB/dz$. The

rescaled Stix functions

$$\begin{matrix} r \\ l \end{matrix} = \pm \frac{\Omega_{c1}\Omega_{c2}}{\omega_{co}} \frac{(\omega \pm \omega_{co})}{(\omega \pm \Omega_{c1})(\omega \pm \Omega_{c2})} \tag{1.3}$$

where v_A is the Alfvén velocity. We have taken the Fourier transform in the direction perpendicular to the magnetic field. In addition, we have rescaled the coordinate variable to some scale length, L_B, which appropriately describes the scale length of the magnetic field.

These equations are related to a dispersion relation which is obtained from the Fourier transform of Eq. (1.1). Indeed, the substitution $i\epsilon d/dz \rightarrow n$ recovers the related dispersion relations

$$n_{\pm}{}^2 = \frac{r+l}{2} - \frac{\kappa^2}{2} \pm \left(\left(\frac{r-l}{2}\right)^2 + \frac{\kappa^4}{4} \right)^{\frac{1}{2}} \tag{1.4}$$

We can make a number of observations concerning the differential Eq. (1.1). These equations are primarily characterized by the quantities ϵ, κ, and the relative spacing of the cyclotron frequencies and the cutoff. The essence of the WKB approximation is contained in the parameter ϵ. For small ϵ the WKB solutions most nearly approximate the correct solution in the regions where r and l are well behaved. The parameter κ, on the other hand characterizes the coupling between the two modes. Indeed, from Eq. (1.1, 1.2) it is obvious that for $\kappa = 0$, the two equations are completely uncoupled and each mode may be described separately. In this case, the equations simply describe the parallel propagating R and L modes.

3 Analytical Considerations

Mode conversion is generally characterized by the coalescence of two propagating modes [*Budden*, 1985; *Fuchs et al.*, 1981; *Swanson*, 1989]. In a region where mode conversion occurs, the propagating modes which coalesce may, in fact, exchange substantial energy. The local properties of a medium in one dimension are characterized by the dispersion relation $D(k, z) = 0$. Saddle points of the dispersion relation where at least two roots coalesce occur where $\partial D/\partial k = 0$ which is satisfied for the mapping $k = k_c(z)$ which depends upon the spatial coordinate, z. At a point, z_b, where the dispersion relation is

satisfied $k_c(z_b)$ becomes a double root of the dispersion relation. The point, z_b, is referred to as a branch point. Near the coupling point, the dispersion equation may be described in terms of an embedded dispersion relation

$$D(k_c, z) + \frac{1}{2}(k - k_c)^2 D_{kk}(k_c, z) = 0 \tag{1.5}$$

Then a differential equation describing the two mode coupling may be obtained from the Fourier transform in k so that

$$\psi''(z) + Q(z)\psi = 0 \tag{1.6}$$

with $Q(z) = -2D(k_c, z)/D_{kk}(k_c, z)$. By definition, the potential Q vanishes at branch points z_b where $D = 0$. When coupling points are well separated, the embedded equation contains sufficient information to describe the coupling between the embedded modes. Such coupling is typically very strong if the coupling point z_b occurs close to the real axis and is weak if the coupling point is far from the real axis.

The particular dispersion relation that we are considering for low frequency waves may be obtained from the Fourier transform of Eq. (1.1)

$$D(k, z) = (k^2 - r)(k^2 - l) + \kappa^2(k^2 - \frac{r + l}{2}) \tag{1.7}$$

where it is understood that r and l are explicit functions of z. The saddle points are located along contours

$$k_c(z) = 0, \frac{1}{2}(r + l - \kappa^2) \tag{1.8}$$

The branch points in space related to these saddle points may be obtained by solving the dispersion relation (1.7) along the saddle point contours, $k_c(z)$. For the coupling point at $k_c = 0$ we find the cutoff condition

$$rl = \frac{\kappa^2}{2}(r + l) \tag{1.9}$$

which occurs at the position at which the magnetic field satisfies the condition

$$\omega^2 = \omega_{co}^2 \omega_{ii}^2 \frac{1 - \kappa^2/2}{\omega_{ii}^2 - \kappa^2 \omega_{co}^2/2} \tag{1.10}$$

This is simply the cutoff condition for the dispersion relation. For small values of κ, this cutoff occurs at the cutoff frequency, ω_{co}, which for parallel propagation is the cutoff of the LHCP L-mode. Near $\kappa^2 = 2$ the denominator diverges. (Actually the root approaches the lower hybrid frequency, but our approximations, suitable for low frequencies do not adequately describe this.) On the other hand, for $\kappa > \sqrt{2}$ a cutoff appears at low frequencies which increases as a function of κ up to the ion-ion resonance. At some critical κ the cutoff passes through the resonance.

The coupling point $k_c = (r + l - \kappa^2)/2$, when substituted into the dispersion relation, yields the condition

$$d^2 + \frac{\kappa^4}{4} = 0 \tag{1.11}$$

where d is the difference function

$$d = \frac{r - l}{2} = \frac{\Omega_{c1}\Omega_{c2}}{\omega_{co}} \frac{\omega(\omega^2 - \omega_{cr}^2)}{(\omega^2 - \Omega_{c1}^2)(\omega^2 - \Omega_{c2}^2)} \tag{1.12}$$

This condition simply corresponds to a double root of the dispersion relation for the modes given in Eq. (1.4). For $\kappa = 0$, this condition is satisfied at the cutoff and crossover frequencies which are the zeros of the function d. As $\kappa \to \infty$, this condition may only be satisfied near the ion gyrofrequencies. For $\kappa \neq 0$ it is clear that this condition may be satisfied only for values of complex d which correspond to complex values of the magnetic field in which case the branch points, z_b, are complex. It should also be clear from the complex conjugate of Eq. (1.11) that the complex branch points always occur in complex conjugate pairs. In Figure 2 we plot values of the complex frequency along which Eq. (1.11) is satisfied. Eq. (1.11) is an eighth order equation in frequency with four complex conjugate pair solutions except at $\kappa = 0$ and $\kappa \to \infty$ where the modes coalesce into a pair of real double roots. For reasonable ionospheric values of the oxygen density, the crossover frequency connects to the oxygen cyclotron frequency and the double root at $\omega = 0$ connects to the heavy ion gyrofrequency. From the topology, we expect coupling to be largest when the coupling points lie near the real axis. In this sense, we see that the largest coupling takes place for small values of κ near the crossover frequency and near the $\omega = 0$ root (which corresponds physically to very low altitudes). On the other hand, for large values of κ the coupling occurs near the two gyrofrequencies (the other gyrofrequency

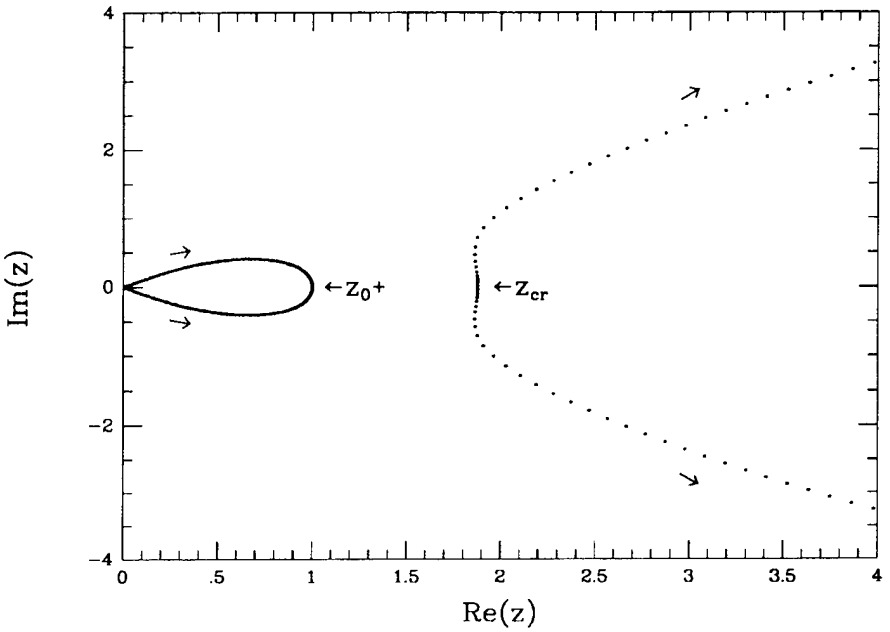

Figure 2: The locus of solutions to Eq. (1.11) for varying κ. The coordinate z corresponds to the ratio ω/Ω_{c1}. For $\kappa = 0$, the condition is satisfied at crossover frequency and at zero frequency while for large values of κ the condition is satisfied near the oxygen resonances and the hydrogen resonance (not shown). The arrows indicate the direction of increasing κ. For very small densities (less than 0.2%) the topology changes and the crossover frequency is connected to the oxygen gyrofrequency whereas the zero frequency solution is connected to the hydrogen gyrofrequency.

at $z = 16$ is not shown in Figure 1.2). The topology of these branch points is discussed in detail by *Le Quéau and Roux* [1992].

In the following sections we will carefully consider the problem at hand, and using suitable approximations, we will extract the behavior of the coupling coefficients analytically. In part 2 of this report, we solve the differential Eq. (1.1) numerically and obtain coefficients valid for all relevant κ.

3.1 Mode Coupling at Crossover Frequency

For $\kappa \ll 1$, the two modes coalesce near the crossover frequency and couple strongly. We may describe this coupling in a number of ways. In doing so,

we shall demonstrate that a substantial amount of energy will be exchanged between the two propagating modes near the crossover frequency for $\kappa \ll 1$. For $\kappa > 1$ the magnetosonic mode is cut off at the lower hybrid frequency which lies above the light ion cyclotron frequency so that only two modes propagate near the heavy ion gyrofrequency. The character of the problem therefore changes as the value of κ changes across some critical value. In this section, we will concentrate on values of κ below this critical value such that four modes propagate in the vicinity of the heavy ion gyroresonance. In a later section, we address propagation for larger values of κ.

One way in which to understand coupling near the crossover frequency is to consider a perturbation about parallel propagation [*Johnson et al.*, 1989; *Budden*, 1985]. Such an analysis is particularly insightful because it is then quite clear that the coupling results from the presence of finite κ. Indeed, the coupling between the two modes is found from Eq. (1.1) to be of order κ^2.

For small κ the fields may be expanded

$$E_{\pm} = E_{\pm}^{(0)} + \kappa^2 E_{\pm}^{(1)} + \ldots \tag{1.13}$$

Eq. (1.1) then reduces to a hierarchy of second order differential equations which are coupled by the known lower order fields. The zeroth order solutions are the two uncoupled parallel propagating R,L-modes. The higher order fields may be determined using variation of parameters. In order to determine the behavior of a downcoming ion-cyclotron (magnetosonic) wave, we must prescribe that $E_{-}^{(0)}$ ($E_{+}^{(0)}$) vanishes. In either case the first order solution for the coupled magnetosonic (ion-cyclotron) wave is found to have the amplitude

$$A(z) = \frac{1}{4i\epsilon}\int_h^z ds[l(s)r(s)]^{-1/4}\exp\left(-\frac{i}{\epsilon}\int_h^z([r(q)]^{1/2} - [l(q)]^{1/2})dq\right) \tag{1.14}$$

where h is some suitably chosen reference altitude above the coupling region. The amplitude of the coupled wave, A, involves an integral over a rapidly oscillating function with scale length ϵ. The integral over such a function is asymptotically small except in the region where the oscillations become stationary. Therefore, coupling between the modes is negligible except at the stationary point where the integrand in the exponential vanishes. The function, A, has a a stationary point at the crossover frequency, ω_{cr}, where

$d = 0$. Because the contribution to the overall integral in (1.14) is exponentially small except near the stationary point, we may expand the integral in the integrand of (1.14) about the stationary point and evaluate it using the standard methods of stationary phase [*Bender and Orszag*, 1978]. The overall integration may then be extended to $+\infty$ which introduces only exponentially small errors. Then we find that the coupling coefficient, up to an unimportant phase, is given by

$$A(-\infty) = \frac{1}{4\epsilon[r(\omega_{cr})]^{1/2}} \int_{-\infty}^{+\infty} ds \exp\left(\frac{-id'(\omega_{cr})s^2}{2\epsilon[r(\omega_{cr})]^{1/2}}\right) \tag{1.15}$$

where

$$d'(\omega = \omega_{cr}) = \frac{2\omega_{cr}^3 \Omega_{c1} \Omega_{c2}}{\omega_{co}(\Omega_{c1}^2 - \Omega_{c2}^2)^2} \frac{(n_1 + n_2)^2}{n_1 n_2} \tag{1.16}$$

The integral may then be rotated in the complex plane in which case it becomes a trivial Gaussian integral. We have thus obtained, to first order in κ the asymptotic form of the coupling to the LHCP mode.

By comparing the Poynting flux along the magnetic field

$$\hat{z} \cdot \mathbf{S} \sim \hat{z} \cdot \mathbf{E} \times \mathbf{B} \sim \Im(E_+^* E'_+ + E_-^* E'_-) \tag{1.17}$$

of the incident wave above the coupling region to that of the coupled wave below the coupling region we may obtain the coupling coefficient

$$C \equiv b \left| \frac{\hat{z} \cdot \mathbf{S}_{below}}{\hat{z} \cdot \mathbf{S}_{above}} \right| = \left. \frac{\pi}{8\epsilon} \frac{\kappa^4}{\sqrt{r} d'} \right|_{\omega = \omega_{cr}} \sim \frac{k_\perp^4}{k_{||}^4} L_B k_{||} \tag{1.18}$$

This result may be naturally extended to larger values of κ if we consider the embedded dispersion relation discussed in Eq. (1.7). The coupling which occurs at the crossover frequency arises from the branch point which is the solution to Eq. (1.11). As discussed previously, two of the solutions to this equation correspond to two complex conjugate roots which occur near the crossover frequency. Moreover, the coupling may be described in terms of the embedded Eq. (1.6) with

$$Q(z) = \frac{1}{2} \frac{d^2 + \kappa^4/4}{2s - \kappa^2} \tag{1.19}$$

The function d has a zero at the crossover frequency, so that locally $d = d_{cr} + d'_{cr}\xi$ with $d_{cr} = 0$. The coupling is described by the potential equation

$$\psi''(\xi) + \frac{1}{2}\frac{d'^2_{cr}\xi^2 + \kappa^4/4}{2s_{cr} - \kappa^2}\psi = 0 \tag{1.20}$$

where the sum function has been evaluated at the crossover frequency (the shape of the potential is not affected too much by the expansion of s, and in particular the complex turning points are independent of the form of s). Eq. (1.20) then takes the form of a Weber equation. The transmission coefficient for this equation is well known [*Heading*, 1962; *Lashmore-Davies et al.*, 1985; *Fuchs et al.*, 1985] and takes the form

$$T = \exp\left(-\frac{\pi}{8\epsilon}\frac{\kappa^4}{d'_{cr}\sqrt{s_{cr} - \kappa^2/2}}\right) \tag{1.21}$$

For small values of κ, $T \approx 1 - C$ as obtained in Eq. (1.18).

As is clear from the preceding analysis, the coupling occurs as the result of finite κ and increases rapidly for small angles of propagation. For larger κ, the coupling approaches unity which means that a complete transfer of power from the predominately RHCP to the predominately LHCP mode occurs. For infinite magnetic field scale length $\epsilon \to 0$ so that coupling is complete except at $\kappa = 0$. In other words, waves propagate as if they remain on their appropriate dispersion surface and do not couple to the other surface except for parallel propagation. In that sense, the scale length determines the strength of the coupling, and provides a criterion for the validity of ray-tracing in the plasma.

3.2 Tunneling Phenomena

The dispersion relations for the propagating modes of the differential Eq. (1.1) are characterized by various cutoffs ($k \to 0$) and in particular by a cutoff-resonance gap. For parallel propagation, the modes are uncoupled and the LHCP ion-cyclotron exhibits the characteristics of the "gap" while the RHCP magnetosonic branch remains essentially constant. The LHCP branch is characterized by the dispersion relation $n_- = l$ where l has a zero at the cutoff frequency, ω_{co}, and a resonance at the heavy ion gyrofrequency,

Ω_{c1}. For non-parallel propagation the situation is more complex in that the refraction indices, $n_{\pm}$, suffer a discontinuity at the gyrofrequency where l diverges. Across this discontinuity, l varies as $1/\omega - \Omega_{c1}$ which changes sign. Hence, although the magnetosonic solution appears to be continuous across the resonance, there is in fact a change in branch $n_{\pm} \rightarrow n_{\mp}$. The existence of such a discontinuity signals one of the most critical aspects of the problem which we are considering to which we shall return many times. Namely, the solution is not continuous, is multivalued, and is characterized by a branch cut. We must work to carefully understand both the physics and mathematics involved in the multivalued nature of the solution and realize that the proper choice of the branch of this solution is essential to our analysis. The proper continuation of the dispersion relation is such that the magnetosonic branch is **not** continuous across the resonance. Hence, although the ion-cyclotron branch apparently mode converts into the magnetosonic branch, the asymptotic behavior of the ion-cyclotron branch below the resonance is determined primarily by the asymptotic behavior of the ion-cyclotron branch above the resonance.

The existence of a "gap" in the dispersion relation indicates that the WKB solutions for a particular mode are cut off and are decaying exponentials over some region of space. In general, the solutions of the dispersion relation across this "gap" decay such that only exponentially small amplitude may be found on the other side of the "gap." In such a case, the mode will have been reflected. However, if the "gap" is sufficiently small such that it is only a fraction of a wavelength in size, substantial tunneling may occur in which case large wave amplitude will be found on the other side [*Budden*, 1985].

The existence of a pole in the differential equation is troublesome in that it is not physically correct, and, in addition, it involves the complications of a regular singular point which generally leads to multivalued solutions of a differential equation except under extraordinary circumstances. As far as physical correctness is concerned, it is obvious that a higher order expansion of the Z-functions in terms of the thermal velocity will introduce corrections to the dispersion relation that will remove the singularity (the Z-functions are well defined at the plasma resonance, hence the corresponding differential equation is also well defined). These corrections arise in the form of a higher order terms in the differential equation which contain the essentials of the physics. Physically, the pole corresponds to dissipation which may be understood in terms of strong ion cyclotron damping. In order to understand

the absorption, we may consider a conserved quantity associated with the differential equation which corresponds to the Poynting flux.

From Eq.. (1.1) and its adjoint, we can form the conserved quantity

$$\mathcal{J} = i(\Psi^{\dagger\prime}\Psi - \Psi^{\dagger}\Psi') \tag{1.22}$$

which is conserved in space according to

$$\mathcal{J}' = i\Psi^{\dagger}(\mathbf{M} - \mathbf{M}^{\dagger})\Psi \tag{1.23}$$

where $'$ denotes real derivatives along a contour with fixed imaginary part (recall that $d\psi^*/dz \neq (d\psi/dz)^*$ except along a line, $z = x + iy$, with y fixed). The conserved quantity, $\mathcal{J}$, corresponds to the Poynting flux along the z-axis, $\hat{z} \cdot (\mathbf{E} \times \mathbf{B})$, and is conserved along the real axis because the functions r and l are real. The function l, however is singular at the heavy ion gyrofrequency so that we expect a discontinuous jump in the value of $\mathcal{J}$ across the singularity. The simplest model which approximates the functions r and l near the resonance and retains the essential characteristics of the dispersion relation is one in which

$$r \approx k_r^2,\ l \approx k_l^2(1 - a/z) \tag{1.24}$$

where a linearized form of the magnetic field, $B = B_0(1 - z)$, has been used. The linearized function, l, retains the resonance and cutoff, while variations in the function, r, are not substantial. The three parameters k_r, k_l, and a may be chosen to retain the location of the crossover, cutoff, and ion-ion frequencies so that the essential characteristics of the dispersion relations are obtained with quantitative accuracy. Near the resonance, the behavior of $\mathcal{J}$ is completely dominated by the singularity in l so that higher order terms in z are unimportant for determining the jump in $\mathcal{J}$ across the cyclotron resonance.

Near the gyrofrequency (z=0), the cold plasma dispersion relations exhibit an unphysical resonance. If we were to incorporate more physical considerations into our analysis, such as the thermal effects, we would find that the solution to the dispersion relation near the gyrofrequencies is of the form $\omega \approx \Omega_{c1} - i\gamma, \gamma > 0$, such that the mode is strongly damped. In light of our approximation for the magnetic field the actual pole should be at a location $\omega - (\Omega_{c1} - i\gamma) = \omega - \omega(1 - z) + i\gamma = 0$, that is, at the location $z = -i\gamma/\omega = -iy$ which lies below the real axis rather than at $z = 0$.

We may determine the discontinuity across the resonance by considering the change in $\mathcal{J}$ along the path $z = x \pm iy$. From Eq. (1.23), the discontinuity is given by

$$\Delta_y = \pm^2 k_l^2 a \int_{-\infty}^{+\infty} \frac{y}{x^2 + y^2} \phi\phi^* \tag{1.25}$$

where ϕ the lower component of Ψ. For small z, ϕ behaves like the Hankel functions or integrals thereof, which are regular [*Abramowitz and Stegun*, 1964], so that the discontinuity is

$$\lim_{y \to 0} \Delta_y = \mp 2\pi k_l^2 a |\phi|^2_{z=0} = \mp\Delta, \ \Delta > 0 \tag{1.26}$$

and represents energy which is absorbed. That is $\mathcal{J}^+ < \mathcal{J}^-$ where the superscript refers to the value along the positive (negative) real axis. If there is no flux in or out on the positive real axis ($\mathcal{J}^+ = 0$) there is a positive energy flow from the left ($\mathcal{J}^- > 0$), which is absorbed. On the other hand, if there is no flux from the left ($\mathcal{J}^- = 0$), then there is a negative flux from the right ($\mathcal{J}^+ < 0$) sending wave energy, which is absorbed, into the system. The value of this energy loss clearly depends on the details of the boundary conditions in that the solution ψ must be known in order to calculate the energy loss. Physically, we may interpret this energy loss as resulting from resonant absorption at the gyrofrequency. Such absorption typically occurs because the cold plasma wave mode converts into a thermal wave which is readily absorbed. Conversely, if the pole lies above the real axis, a similar procedure results in an energy gain which is not physical.

We may obtain a substantial amount of information concerning the asymptotic behavior of the solutions. The WKB solutions in this case are of the form

$$\Theta = \exp\left(\pm \frac{i}{\epsilon} \int^z n_\pm ds\right) \tag{1.27}$$

For large values of z the indices may be expanded using the approximation (1.24) to give

$$n_\pm \approx n_\pm^0 - \frac{k_l^2 a}{4z} \frac{\pm\delta + \sqrt{\delta^2 + \kappa^4/4}}{n_\pm^0 \sqrt{\delta^2 + \kappa^4/4}} \tag{1.28}$$

where

$$n_\pm^0 = \left[\sigma - \frac{\kappa^2}{2} \pm \left(\delta^2 + \frac{\kappa^4}{4}\right)^{\frac{1}{2}}\right]^{1/2} \tag{1.29}$$

and the zero order sum and difference functions are

$$\sigma = \frac{k_r^2 + k_l^2}{2}, \delta = \frac{k_l^2 - k_r^2}{2} > 0 \tag{1.30}$$

so that the four WKB solutions take the form

$$\begin{aligned} \Theta_+^{\pm} &= \exp(\pm i/\epsilon(n_+ z - \beta_+ \log z/2)) \\ \Theta_-^{\pm} &= \exp(\pm i/\epsilon(n_- z - \beta_- \log z/2)) \end{aligned} \tag{1.31}$$

where

$$\beta_{\pm} = \frac{k_l^2 a}{2} \frac{\pm\delta + \sqrt{\delta^2 + \kappa^4/4}}{n_{\pm}^0 \sqrt{\delta^2 + \kappa^4/4}} \tag{1.32}$$

and the coupling is characterized by the multivalued nature of the logarithm.

From these expressions we can determine the transmission coefficients for the case of incident magnetosonic waves or ion-cyclotron waves. We may extend the WKB solutions into the complex plane and use the dominance of the various solutions to determine transmission properties [*Heading*, 1962]. The solutions on the positive real axis are of the form

$$\psi = A\Theta_+^- + B\Theta_-^- + C\Theta_-^+ + D\Theta_+^+, \; Arg(z) = 0 \tag{1.33}$$

where we have written them in order of dominance in the upper half complex plane. The lower component, ϕ, of Ψ is of the same form with coefficients which are related to A, B, C, and D by the dispersion relation. The WKB approximations in the complex plane, however, are at best limited to validity within certain sectors due to the Stokes phenomenon which results from the fact that the exponential solutions are too simple to adequately describe the qualitative behavior of the actual functions. Although the coefficient of the dominant solution within a given region remains unchanged, the subdominant solutions are liable to change. Moreover, on the grounds of continuity we expect that if the coefficient of the more dominant solutions vanish, the coefficient of the most dominant remaining solution is unchanged. To accommodate this change, we make a discontinuous adjustment of the subdominant terms along the Stokes lines where the subdominant terms are least significant. The adjustment should be proportional to the amplitude of the dominant solution so that it will vanish if the dominant solution vanishes. The Stokes lines in this case are along the positive imaginary axis while the

anti-Stokes lines are along the positive real axis. According to the Stokes phenomenon the solution takes the general form

$$\begin{aligned}\psi = \quad & A\Theta_+^- + (B - AS_1)\Theta_-^- + (C - AS_2 - BS_3)\Theta_-^+ \\ & +(D - AS_4 - BS_5 - CS_6)\Theta_+^+, \ Arg(z) = \pi \end{aligned} \tag{1.34}$$

on the negative real axis. We have added Stokes constants across the region of least dominance according to a reasonable prescription which retains the continuity of the equations in the absence of the more dominant solutions. The boundary conditions for downgoing ion-cyclotron waves are given by

$$A = 1, \ B = S_1, \ C = D = 0 \tag{1.35}$$

while for downgoing magnetosonic waves the boundary conditions are

$$A = 0, \ B = 1, \ C = D = 0 \tag{1.36}$$

We may immediately write down the asymptotic form of the transmission coefficients in terms of the logarithmic singularity. The leading order coefficient for downgoing ion-cyclotron waves is given by

$$T_{IC} = \frac{|\Theta_+^-|^2_{Arg(z)=\pi}}{|\Theta_+^-|^2_{Arg(z)=0}} = \mathrm{e}^{-\pi\beta_+/\epsilon} \tag{1.37}$$

whereas for downgoing magnetosonic waves in the absence of an incident ion-cyclotron wave has no transmitted flux in the ion-cyclotron mode and transmission to the magnetosonic mode given by

$$T_{MS} = \frac{|\Theta_-^-|^2_{Arg(z)=\pi}}{|\Theta_-^-|^2_{Arg(z)=0}} = \mathrm{e}^{-\pi\beta_-/\epsilon} \tag{1.38}$$

We can make a number of observations concerning these two results. First, for $\kappa \ll \delta$, we find from Eq. (1.32) that T_{IC} is simply the Budden coefficient described previously. That is $\beta_+ = k_l a(1 - O(\kappa^4))$ which has little dependence on κ, so that transmission for this mode may be considered to be essentially Budden tunneling and should have that character. With increasing κ, the tunneling diminishes. For large κ, we find that the coefficient approaches another constant, namely

$$\beta_+ = \frac{k_l^2 a}{2\sqrt{\sigma}} \tag{1.39}$$

indicative of Budden tunneling for nearly perpendicular propagation near the ion-ion hybrid frequency.

On the other hand, for the downgoing magnetosonic wave we find that for small κ Eq. (1.32) gives an intriguing result. The transmission coefficient then takes the form

$$T_{MS} = \mathrm{e}^{-\pi\beta_-/\epsilon} \approx \exp\left(\frac{k_l^2 a}{\epsilon 16 k_r \delta^2}\kappa^4\right) \tag{1.40}$$

We may relate this transmission coefficient to the coupling coefficient obtained from the saddle point analysis. If we recognize that difference function is of the form

$$d = -\delta + \frac{k_l^2 a}{2z} \tag{1.41}$$

we find that

$$d'_{cr} = \frac{2\delta^2}{k_l^2 a} \tag{1.42}$$

which then demonstrates that the transmission coefficient is the same as the coupling coefficient established in Eq. (1.18). We may make a physical interpretation of this result. For parallel propagation transmission of the magnetosonic mode is complete ($T = 1$). However, coupling increases rapidly with larger values of κ, and we find that the transmission in the magnetosonic mode falls off substantially.

The values of the Stokes constants may not be unambiguously determined using the methods of the previous section although a number of relationships between the amplitudes of the various waves may be determined. For the case of a "large" gap, however, we may actually determine the coefficients unambiguously. In this case the WKB solution, Θ_+^-, has negligible amplitude at $-\infty$, i.e. $\beta_+ \to \infty$ so that there is no transmission in that mode. Furthermore, the restriction that no upgoing ion-cyclotron wave, Θ_+^+, be found at $-\infty$ implies that $\Delta- > 0$ so that no absorption occurs. In this case, after substantial and lengthy algebra detailed in Appendix A, it is possible to show that in the limit of a large "gap" the transmission and reflection coefficients, as defined in the appendix to be the ratio of the Poynting flux of a particular wave to that of the incident wave, are given by

$$\begin{aligned} C_{IC}^T &= 1 - \mathrm{e}^{-\pi\beta_-/\epsilon} = 1 - C \\ R_{IC} &= \mathrm{e}^{-2\pi\beta_-/\epsilon} = C^2 \\ C_{IC}^R &= e^{-\pi\beta_-/\epsilon}(1 - e^{-\pi\beta_-/\epsilon}) = C(1-C) \end{aligned} \tag{1.43}$$

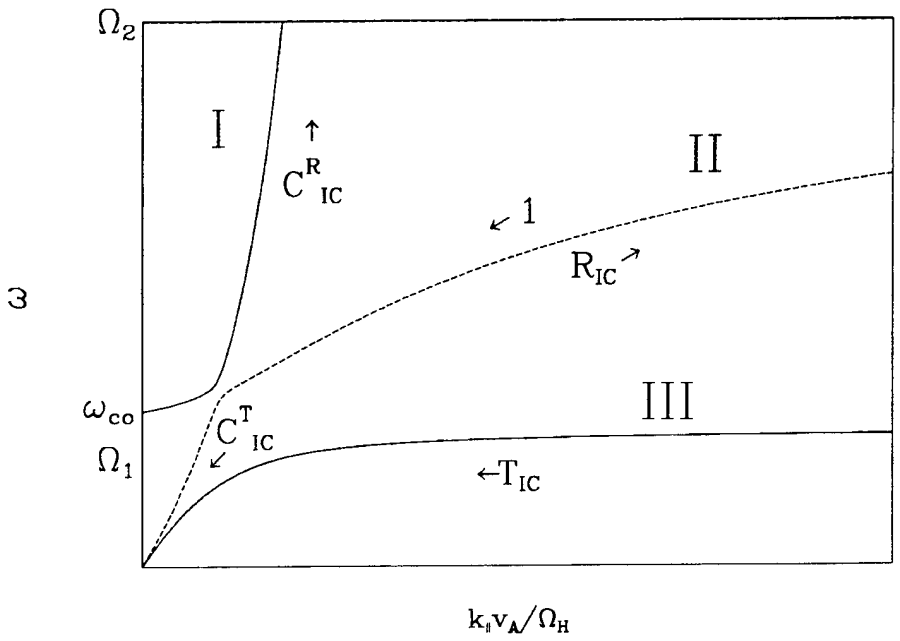

Figure 3: Illustration of the meaning of the coefficients for a downgoing ion cyclotron wave. Waves are reflected back along the two upward propagating modes while a wave is transmitted on the downgoing magnetosonic branch.

where the meaning of the coefficients are illustrated in Figure 3. For a magnetosonic wave incident from above we find that

$$\begin{aligned} T_{MS} &= e^{-\pi\beta_-/\epsilon} = C \\ R_{MS} &= (1 - e^{-\pi\beta_-/\epsilon})^2 = (1 - C)^2 \\ C^R_{MS} &= e^{-\pi\beta_-/\epsilon}(1 - e^{-\pi\beta_-/\epsilon}) = C(1 - C) \end{aligned} \tag{1.44}$$

This process is again illustrated in Figure 4.

As stated previously, in the case of large gap, wave propagation is entirely determined by the interaction at the crossover frequency which, as we have just shown, is characterized by the coefficient $C = e^{-\pi\beta_-/\epsilon}$. In order to understand these results in an intuitive manner, consider the situation of Figure 3. A downgoing ion-cyclotron wave with unit flux encounters the crossover frequency at which point a fraction, C, is transferred from branch II to branch I. A fraction, $1 - C$, continues down along mode II and is the coupled transmission coefficient C^T_{IC}. The wave which couples to branch I reflects at the cutoff frequency and once again encounters the crossover

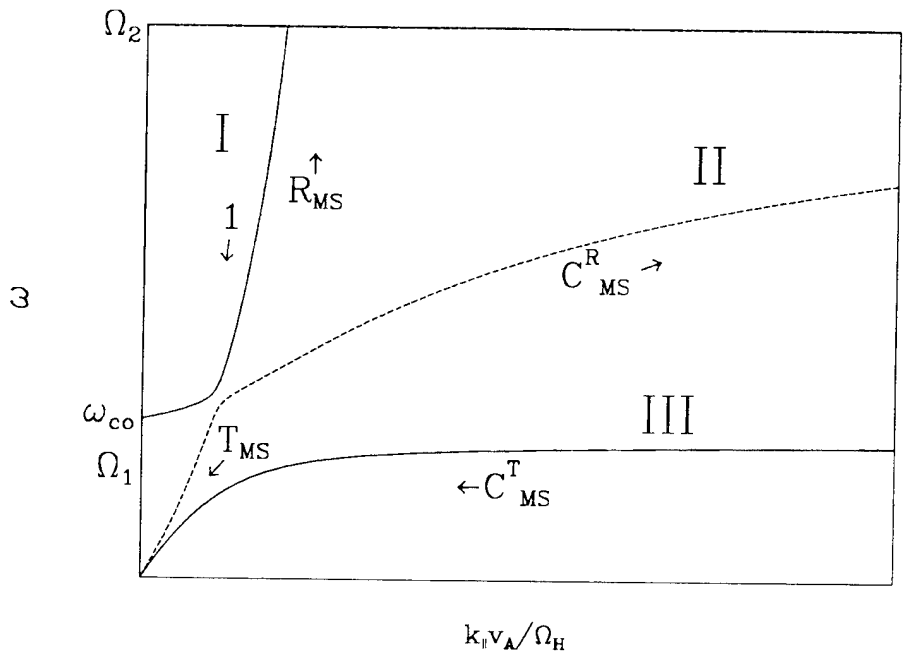

Figure 4: Illustration of the meaning of the coefficients for a downgoing magnetosonic wave. Waves are reflected back along the two upward propagating modes while a wave is transmitted on the downgoing magnetosonic branch.

frequency as an upgoing wave. This reflected wave has amplitude C. Upon coupling, a fraction, C, of this reflected wave flux is coupled to branch II comprising the reflection coefficient $R_{IC} = C^2$. The fraction, $1 - C$, remains on branch I and is the coupled reflected wave $C^R_{IC} = C(1 - C)$. Although in the limit of a small "gap" the transmission coefficient T_{IC} is a Budden tunneling term, in the limit of a large "gap" T_{IC} vanishes.

The case of an incident magnetosonic wave is illustrated in Figure 4. In this case, a magnetosonic wave of unit amplitude is incident along branch I. Coupling occurs at the crossover frequency and a fraction, C, of the incident wave is coupled to branch II and comprises the transmission coefficient, $T_{MS} = C$. The fraction, $1 - C$, remains on branch I, is reflected at the cutoff frequency, and again encounters the crossover frequency as an upgoing wave. The amplitude of this reflected wave is $1 - C$. Again coupling occurs at the crossover frequency and a fraction, C, of the reflected wave is coupled onto mode II giving the coupled reflected wave $C^R_{MS} = C(1 - C)$, and the

remaining wave power, $R_{MS} = (1 - C)^2$ is reflected along branch I. There is no coupled mode C^T_{MS} in the limit of large "gap." As one can see, for the case of a large frequency gap, the coefficients are well described in terms of the coupling at the crossover frequency.

In the case of a small "gap" it is not possible to determine the Stokes parameters unambiguously although a number of relationships between them may be derived using symmetry properties. In the following chapter we will determine the coefficients numerically. The results which we have obtained, however, are useful in that they provide both physical insight and a check of our numerical procedure. The method which we have used for the Budden equation is, however, sufficient to determine the coefficients for large κ in which case only one mode propagates at $\pm\infty$.

An alternate approach which makes use of the Fourier transform of Eq. (1.1) has been presented by *Le Quéau and Roux* [1992]. Their approach is based upon the asymptotic expansion of the integral transform of the approximate solution to the differential equation. The solution is continued into the complex plane much in the manner of the phase integral approach, and they derive the same reflection, coupling and transmission coefficients as detailed above. Their result expands upon the approach detailed above and is useful in the regime in which the "gap" is small. In the limit of a large "gap," the results obtained above are in agreement with their calculations. Furthermore, their results are consistent with the relations that may be derived between the coefficients. Our work substantiates the coefficients which they obtained in an independent manner. The reader is referred to their paper for the complete set of coefficients.

3.3Phase Integral Solution for Large κ—Two Propagating Modes

As one can see from Eq. (1.28), for large enough κ, $\sigma < \kappa^2$, so that two of the solutions become complex. That is, we find that n_+ is real and n_- is imaginary. This means that two of the asymptotic solutions are growing along the real axis (a notably unphysical situation). When this is the case, the positive and negative real axes become Stokes lines for two of the solutions while the positive and negative imaginary axes remain the Stokes lines for the other two solutions. The anti-Stokes lines are to be found asymptotically

along the rays

$$n_+^0 x = \pm n_-^0 y \tag{1.45}$$

where $z = x+iy$ is the complex coordinate. This situation is easier to evaluate because each solution is dominant in one of four sectors in the complex plane.

At this point, we need to consider the concept of Stokes phenomena in somewhat more detail. Tracing Stokes coefficients in reality is only valid in the sense that in the region of maximum dominance, the coefficient of the exponential term must agree with the exact solution in an asymptotic sense. However, we actually require further information concerning the asymptotic behavior of the subdominant terms in order to extract the reflection and transmission coefficients. This information is important because we must determine the value of the oscillatory solutions along the real axis in the presence of an unphysical growing mode.

In previous work [*Johnson*, 1992] we demonstrated using an integral equation, that the Stokes coefficients for the asymptotic solutions of the fourth order equation which we are considering change abruptly at definite values of $Arg(z)$ in the region of maximum subdominance. It would appear that these jumps occur at three distinct values of $Arg(z)$—along the Stokes lines and the bounding anti-Stokes lines of the maximally subdominant region. The change only occurs in the coefficient of the most subdominant solution. We may, therefore, determine the appropriate asymptotic behavior of the solution of interest if the relevant WKB solutions involved in the analysis are not maximally subdominant in the region where they must be evaluated. Because the solutions with growing (decaying) exponential behavior do not contribute to the Poynting flux on the real axis, we need only evaluate the coefficients of the oscillatory solutions in order to determine the transmission and reflection coefficients. The oscillatory solutions are not maximally subdominant along the real axis, and therefore, we may determine the coefficients unambiguously. In order to incorporate the Stokes phenomena we introduce the Stokes multipliers such that upon crossing a Stokes line on which a WKB solution is maximally subdominant the coefficient of that term equals the coefficient before crossing the Stokes lines + $\sum_j S_j \times$ the coefficients of the jth dominant term on the Stokes line [*Heading*, 1957; *Budden*, 1985].

Appropriate boundary conditions require that at $\pm\infty$ the exponentially growing modes be absent. In addition, appropriate boundary conditions require that no upgoing wave be found at $-\infty$. In order to satisfy these

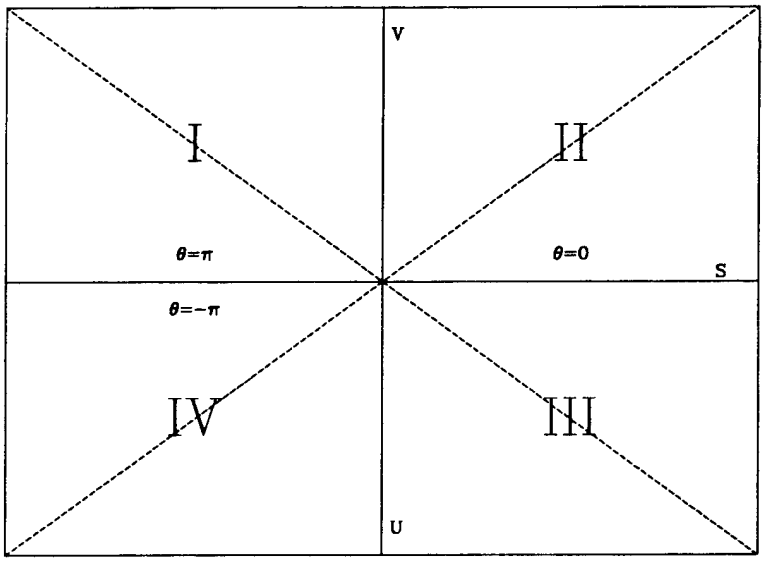

Figure 5: Sectors of the complex plane divided according to regions of dominance and subdominance of the asymptotic WKB solutions. The Stokes lines and anti-Stokes lines are solid and dashed respectively.

conditions, we assume along or above the positive real axis that the solution takes the form

$$\psi = A\Theta_+^- + B\Theta_-^- + C\Theta_-^+ + D\Theta_+^+, \quad \text{Region II} \tag{1.46}$$

Using the rules stated above we may continue the solution into the following sectors illustrated in Figure 5.

$$\psi = A\Theta_+^- + B\Theta_-^- + C'\Theta_-^+ + D\Theta_+^+, \quad \text{Region III} \tag{1.47}$$

with

$$C' = C - AS_1 - BS_2 - DS_4 \tag{1.48}$$

$$\psi = A'\Theta_+^- + B\Theta_-^- + C'\Theta_-^+ + D\Theta_+^+, \quad \text{Region IV} \tag{1.49}$$

with

$$A' = A - BU_2 - C'U_3 - DU_4 \tag{1.50}$$

and

$$\psi = A\Theta_+^- + B\Theta_-^- + C\Theta_-^+ + D'\Theta_+^+, \quad \text{Region I} \tag{1.51}$$

with

$$D' = D + AV_1 + BV_2 + CV_3 \tag{1.52}$$

where S, U, and V are Stokes constants. In order to satisfy the boundary conditions for downgoing waves, we require that

$$B = C = D' = 0, \; A = 1 \tag{1.53}$$

Then we may immediately write down the transmission and reflection coefficients

$$T_{IC} = \frac{|\Theta_+^-|^2_{Arg(z)=pi}}{|\Theta_+^-|^2_{Arg(z)=0}} = \mathrm{e}^{-\pi\beta_+/\epsilon} \tag{1.54}$$

and

$$R_{IC} = \frac{|\Theta_+^+|^2_{Arg(z)=0}}{|\Theta_+^-|^2_{Arg(z)=0}}|V_1|^2 = |V_1|^2 \tag{1.55}$$

In order to determine the Stokes constant V_1 we may consider the situation with $B = C = D = 0, A = 1$ from which we can compute the Stokes constant if we again invoke the conservation law. As it turns out, on the real axis, the exponentially growing solutions do not contribute to the Poynting flux so that the conserved quantity $\mathcal{J}/n_+$ is found to be

$$\mathcal{J}/n_+ = \begin{cases} 1 & Arg(z) = 0 \\ \mathrm{e}^{\pi\beta_+/\epsilon} & Arg(z) = -\pi \\ \mathrm{e}^{-\pi\beta_+/\epsilon} - |V_1|^2\mathrm{e}^{\pi\beta_+/\epsilon} & Arg(z) = \pi \end{cases} \tag{1.56}$$

Once again, from the energy discontinuity

$$-\Delta = 1 - \mathrm{e}^{\pi\beta_+/\epsilon} = -1 + \mathrm{e}^{-\pi\beta_+/\epsilon} - |V_1|^2\mathrm{e}^{\pi\beta_+/\epsilon} \tag{1.57}$$

we obtain the Budden-like reflection coefficient

$$R_{IC} = |V_1|^2 = (1 - T_{IC})^2 \tag{1.58}$$

3.4 Mode Coupling at Low Frequencies, Large κ

The result which we have just obtained for large values of κ does not depend critically on the crossover frequency in that the factor β_+ depends weakly on the location of the crossover frequency. From the analysis described in Section 3.1, we find that for large values of κ, the saddle point associated with the crossover frequency is located far from the real axis and is near the hydrogen cyclotron frequency. As a result, coupling is not strongly dependent upon the location of the saddle point associated with the crossover frequency. However, in Figure 2, we find that the coupling point associated with zero frequency at small κ, approaches the oxygen resonance for large values of κ and is therefore of primary interest. As described previously, the transition from four propagating modes to two propagating modes occurs at a critical value of κ. Assuming that r and l take a simple form such as in Eq. (1.24), the cutoff condition (1.9) implies that

$$z_{co} = a\frac{1 - \kappa^2/4k_r^2}{1 - \sigma\kappa^2/k_r^2k_l^2} \tag{1.59}$$

We then find that the abrupt change in the behavior of the modes occurs at the critical value

$$\kappa^2 = \frac{k_r^2k_l^2}{\sigma} \tag{1.60}$$

For values smaller than this value of κ, the mode conversion processes are determined primarily from the coupling point associated with the crossover frequency. For intermediate values of κ, $k_r^2k_l^2/\sigma < \kappa^2 < 2k_r$, four modes propagate in the vicinity of the heavy ion resonance although the magnetosonic branch is cut off at some point below the gyrofrequency and does not propagate above the gyrofrequency. In this case, the dominant saddle point is that associated with zero frequency at small κ and the oxygen resonance at large κ. For larger κ, $\kappa^2 > 2k_r$, the downgoing ion-cyclotron wave is cutoff above the oxygen resonance at a frequency which approaches the ion-ion hybrid frequency and only two modes propagate. In this case the transmission properties may be obtained by expanding about the coupling point associated with the cutoff condition $rl - \kappa^2 s = 0$. In the ensuing analysis we will follow the reasoning of *Lashmore-Davies et al.* [1985] and *Fuchs et al.* [1985], and we will consider the cases of intermediate and large κ separately.

The expression for the location of the saddle point in the complex plane is, as before, given by Eq. (1.11) As discussed in Section 3.1, the solutions to

this condition are complex conjugate pairs which satisfy a quartic equation as plotted in Figure 2. In this case the potential again takes the form (1.19). The fact that the roots occur in complex conjugate pairs means that the function, $d^2 + \kappa^4/4$, will have the form of a complex conjugate barrier equation described by the Weber equation. It is once again both tractable and somewhat reasonable to assume the form of r and l as assumed in Eq. (1.24). In this case, the potential takes the form

$$Q(\xi) = \frac{\delta^2 + \kappa^4/4}{4\xi^2(s - \kappa^2/2)} \left((\xi - \xi_r)^2 + \xi_i^2\right) \tag{1.61}$$

where

$$\xi = \xi_r \pm \xi_i = \frac{k_l^2 a}{2} \frac{\delta \pm i\kappa^2/2}{\delta^2 + \kappa^4/4} \tag{1.62}$$

is the location of the complex conjugate roots (for large κ the imaginary part dominates as is the case for the actual solutions to the third-order equation). Once again the essential asymptotic features of the embedded dispersion relation are retained if we evaluate the constant factor in Eq. (1.61) at some convenient point, such as the real frequency above. If we then make the judicious choice for the variables

$$k_0^2 = \frac{\delta^2 + \kappa^4/4}{\xi_r^2(s_r - \kappa^2/2)} \tag{1.63}$$

and

$$\beta = \frac{\xi_i}{2} = \frac{k_l^2 a}{2(\delta^2 + \kappa^4/4)} \frac{\kappa^2}{4} \tag{1.64}$$

(where the index r indicates that the function is to be evaluated at ξ_r) then the embedded equation is of the form of the Weber equation which has the transmission coefficient [*Lashmore-Davies et al.*, 1985; *Fuchs et al.*, 1985]

$$T = \mathrm{e}^{-2\pi k_0 \beta^2/\epsilon} \tag{1.65}$$

where the argument of the exponential takes the form

$$k_0\beta^2 = \frac{k_l^2 a}{8} \frac{\kappa^4/4\delta}{\sqrt{(\delta^2 + \kappa^4/4)(\kappa^4/4\delta + \kappa^2/2 - k_r^2)}} \tag{1.66}$$

Near the upper limit of validity, the two results have a reasonably simple limit. For $\kappa^2/2 = k_r^2$

$$\beta_+ = \frac{k_l^2 a}{2\sqrt{\delta^2 + k_r^4}} \tag{1.67}$$

whereas the equivalent coefficient from the saddle point becomes

$$2k_0\beta^2 = \beta_+ \frac{k_r^2}{2\sqrt{\delta}} \tag{1.68}$$

yielding roughly the same expression. Over the range of densities for which absorption is strong (0.5-5%), the ratio, $k_r^2/2\sqrt{\delta}$ takes values ranging from 1.3 to 0.6 depending on the density ratio and the two results are in reasonable agreement. Hence, we can understand that the coupling which arises at low frequencies results from coupling at the saddle point which occurs near the oxygen resonance for large values of κ.

The form of the reflection coefficient may be understood physically in the same manner that we understood coupling for smaller κ. In this case, coupling between the modes occurs below the heavy ion gyrofrequency. As illustrated in Figure 6, incident waves along mode II couple at the complex coupling point. A fraction, $T_{IC} = T = \mathrm{e}^{-\pi\beta_+}$, is transferred to branch III. The remaining wave energy, $1 - T$, continues along branch II, is reflected at the cutoff frequency for mode II and once again encounters the coupling point. The two waves couple again and a fraction, $1 - T$, of the remaining wave power is found on branch II giving the reflection coefficient, $R_{IC} = (1 - T)^2$. The rest of the wave power is absorbed at the resonance.

For larger values of κ we must expand about the cutoff-resonance pair which arises near the ion-ion hybrid frequency. In this case the coupling potential in (1.6) takes the form

$$Q = \frac{rl - \kappa^2 s}{r + l - \kappa^2} \tag{1.69}$$

Once again, the functions may be expanded about the gyrofrequency, $\Omega_{c1} = \omega(1 - z)$. After suitable definitions and algebraic manipulation detailed in Appendix B, the potential is found to take the Budden form

$$Q = k_0^2(1 - \alpha/z) \tag{1.70}$$

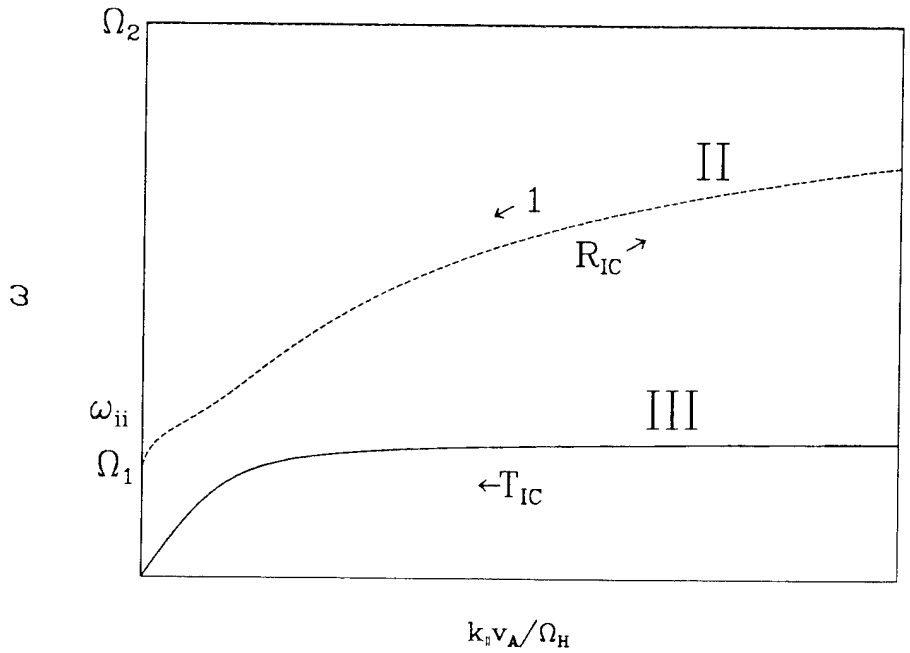

Figure 6: Illustration of the physical meaning of the coefficients for a downgoing ion-cyclotron wave for large angle of propagation. Waves are transmitted onto mode III and reflected back along mode II.

The transmission coefficients for the Budden equation are well known

$$T = \mathrm{e}^{-\pi k_0 \alpha/\epsilon}, \quad R = (1-T)^2 \tag{1.71}$$

In the limit of large κ the potential takes the form

$$Q \approx s = -\frac{\Omega_{c1}^2 \Omega_{c2}^2}{\omega_{ii}^2} \frac{(\omega^2 - \omega_{ii}^2)}{(\omega^2 - \Omega_{c1}^2)(\omega^2 - \Omega_{c2}^2)} \tag{1.72}$$

which exhibits a cutoff at the ion-ion hybrid frequency and a resonance at the oxygen gyrofrequency. Expanding s about the gyrofrequency

$$s \approx \sigma(1 - k_l^2 a/2\sigma z) \tag{1.73}$$

we find that the coefficient takes the form

$$k_0 \alpha = \beta_+ = \frac{k_l^2 a}{2\sqrt{\sigma}} \tag{1.74}$$

in agreement with (1.39) of the previous section.

Comparing both this result and the result for intermediate κ, we find that both coefficients are of the Budden form with transmission and reflection coefficients given by T and $(1-T)^2$ respectively. These results compare well with the form (1.54, 1.58) which we obtained using the phase-integral analysis. In this analysis, we have three parameters: k_r, k_l and a. These three parameters are sufficient to retain the location of the resonance (Ω_{c1}), crossover frequency (ω_{cr}), cutoff frequency (ω_{co}), and ion-ion hybrid frequency (ω_{ii}). Thus, in some sense we can form a uniform approximation which retains the characteristics of the crossover and cutoff frequencies for small κ but retains the characteristics of the ion-ion hybrid resonance for perpendicular propagation. This linear approximation is good if the coupling is dominated by one or the other of the two coupling points, but if both coupling points are of significant importance, one suspects that the linear approximation will fail for the phase-integral approach.

4 Summary

In this report we have explored the analytic properties of the mode conversion processes. We have found that near the crossover-cutoff-resonance triplet the propagating modes couple strongly, and substantial energy may be exchanged between modes. For small values of κ, we have determined that the ion-cyclotron mode tunnels in a manner described by the Budden equation, and substantial wave power will be transmitted and absorbed for nearly parallel propagation. We have also shown that this tunneling factor drops off with larger κ, vanishing as κ becomes the order of 1 (in which case the approximation is not valid). For larger angles of propagation, this mode continues to be characterized by Budden tunneling; however, in this case, the mode does not interact with the nonpropagating magnetosonic wave. For large angles of propagation, the mode is described by a simple expression for tunneling at the ion-ion hybrid resonance. Because the "gap" which characterizes this tunneling is smaller than that for parallel propagation, we expect that the tunneling and absorption will be of the same order as for parallel propagation.

Incident magnetosonic waves are only of interest for reasonably small κ because for larger κ they do not propagate. For parallel propagation the

coupling is negligible and the mode propagates without much interaction. However, the coupling increases rapidly as κ^4. For large κ the coupling is reasonably complete and all the wave power is reflected. The reflection occurs because the magnetosonic mode couples completely to the LHCP wave which is cut off far above the oxygen resonance so that the tunneling barrier becomes insuperable.

In the rest of this report, we explore the numerical value of these coefficients. In particular, we will solve the differential equations numerically in the regimes where we have not obtained the coefficients. As we shall demonstrate, the basic features of the analytical results are retained.

5 Appendix A: Coefficients for a Small "Gap"

In this appendix we consider the linear approximation in the limit of a small "gap." Given the linear approximations (1.24), the solutions of (1.1) may be decomposed into the appropriate WKB solutions (1.27) far from the coupling region. Along the positive (negative) real axis, the solutions are of the form (1.33) and (1.34) respectively. A large energy gap implies that $\Delta = 0$ if the ion-cyclotron wave is not found below the coupling region. In the asymptotic regime along the real axis, the conserved flux is of the form

$$f_+|A|^2 e^{-\eta_+} + f_-|B|^2 e^{-\eta_-} - f_-|C|^2 e^{\eta_-} - f_+|D|^2 e^{\eta_+} \qquad (1.A1)$$

while along the positive real axis, it takes the form

$$f_+|A|^2 + f_-|B + S_1 A|^2 - f_-|C + S_2 A + S_3 B|^2 - f_+|D + S_4 A + S_5 B + S_6 C|^2 \quad (1.A2)$$

where the constants $f_\pm$ are factors which relate the lower and upper components, ψ and ϕ, of the differential Eq. (1.1)

$$f_\pm = n_\pm \left[1 + \left(\frac{2}{\kappa^2}(n_\pm^2 - r + \kappa^2/2)\right)^2\right] \qquad (1.A3)$$

and

$$\eta_\pm = \pi\beta_\pm \qquad (1.A4)$$

A large "gap" implies that η_+ is very large.

5.1 Magnetosonic Wave

The boundary conditions for a downgoing magnetosonic wave are

$$A = 0,\ B = 1,\ C = 0,\ D = 0 \tag{1.A5}$$

for which we find

$$\mathcal{J} = \begin{cases} f_- - f_-|S_3|^2 - f_+|S_5|^2 & Arg(z) = 0 \\ f_-\mathrm{e}^{-\eta_-} & Arg(z) = \pi \end{cases} \tag{1.A6}$$

Because $\Delta = 0$ the ratios of these terms correspond to the coefficients. Thus,

$$T_{MS} = \mathrm{e}^{-\eta_-},\ R_{MS} = |S_3|^2,\ C^R_{MS} = \frac{f_+}{f_-}|S_5|^2 \tag{1.A7}$$

A suitable choice of three other boundary conditions is sufficient to determine the Stokes coefficients, $|S_3|$, $|S_5|$ and $|S_6|$. We find that

$$\begin{aligned} |S_6|^2 &= \frac{f_-}{f_+}(\mathrm{e}^{\eta_-} - 1) \\ |S_5|^2 &= \frac{f_-}{f_+}\mathrm{e}^{-\eta_-}(\mathrm{e}^{-\eta_-} - 1) \\ |S_3|^2 &= (\mathrm{e}^{-\eta_-} - 1)^2 \end{aligned} \tag{1.A8}$$

so that

$$T_{MS} = \mathrm{e}^{-\eta_-},\ R_{MS} = (1 - \mathrm{e}^{-\eta_-})^2,\ C^R_{MS} = \mathrm{e}^{-\eta_-}(1 - \mathrm{e}^{-\eta_-}) \tag{1.A9}$$

5.2 Incident Ion-Cyclotron Wave

The boundary conditions for an ion-cyclotron wave are

$$A = 1,\ B = S_1,\ C = 0,\ D = 0 \tag{1.A10}$$

for which we find

$$\mathcal{J} = \begin{cases} f_+ - f_-|S_2 + S_1S_3|^2 - f_+|S_4 + S_1S_5|^2 & Arg(z) = 0 \\ f_-|S_1|^2\mathrm{e}^{-\eta_-} & Arg(z) = \pi \end{cases} \tag{1.A11}$$

where it is to be noted that we have ignored the term with the factor $e^{-\eta_+}$ along the negative real axis in that it is exponentially small. We may then identify the coefficients to be the ratios of the downgoing fluxes to the incident flux

$$C_{IC}^T = \frac{f_-}{f_+}|S_1|^2 e^{-\eta_-},\ C_{IC}^R = \frac{f_-}{f_+}|S_2 + S_1 S_3|^2,\ R_{IC} = |S_4 + S_1 S_5|^2 \quad (1.A12)$$

It is possible to determine a relationship between the remaining Stokes constants, $|S_1|$, $|S_2|$, and $|S_4|$ from three different boundary conditions

$$\begin{aligned} |S_2|^2 &= \frac{f_+}{f_-}(e^{\eta_-} - 1)|S_4|^2 \\ |S_1|^2 &= \frac{f_+}{f_-}(e^{\eta_-}|S_4|^2 - 1) \end{aligned} \quad (1.A13)$$

In order to make further progress, let us consider the case

$$A = 1,\ B = S_1,\ C = S_2 + S_1 S_3,\ D = 0 \quad (1.A14)$$

for which we find

$$\mathcal{J} = \begin{cases} f_+ - f_+|\chi|^2 & Arg(z) = 0 \\ f_-|S_1|^2 e^{-\eta_-} - f_-|S_2 + S_1 S_3|^2 e^{\eta_-} & Arg(z) = \pi \end{cases} \quad (1.A15)$$

where we have defined $\chi = S_4 + S_1 S_5 + (S_2 + S_1 S_3)$. To extract the value of χ, we may consider the case with $D = \chi$ with A, B and C as in (1.A14). Because Θ_+^- is maximally subdominant in the lower half plane we may, in fact, determine the value of the solution at $Arg(z) = -\pi$. The coefficient of the maximally subdominant solution must remain unchanged in the absence of any of the more dominant solutions so that

$$\mathcal{J} = \begin{cases} f_+ & Arg(z) = 0 \\ f_+ e^{\eta_+} & Arg(z) = -\pi \\ f_+ e^{-\eta_+} + f_-|S_1|^2 e^{-\eta_-} & Arg(z) = \pi \\ -f_-|S_2 + S_1 S_3|^2 e^{\eta_-} - f_+|\chi|^2 e^{\eta_+} & \end{cases} \quad (1.A16)$$

where we have explicitly kept the dependence of η_+. Moreover, we realize that for this situation Δ rather than vanishing takes a large value. For the case of non-zero Δ the conservation law yields

$$\begin{aligned} \Delta &= f_+(e^{\eta_+} - 1) \quad (1.A17) \\ &= f_+(1 - e^{-\eta_+} + |\chi|^2 e^{\eta_+}) + f_-(|S_2 + S_1 S_3|^2 e^{\eta_-} - |S_1|^2 e^{-\eta_-}) \end{aligned}$$

In the limit of large η_+, we realize that the Stokes constants which appear in the equation are finite so that

$$|\chi|^2 = 1 \tag{1.A18}$$

Then, we determine from Eq. (1.A15) that

$$|S_2 + S_1 S_3|^2 = |S_1|^2 e^{-2\eta_-} \tag{1.A19}$$

Finally, two more boundary conditions yield an equation relating $|S_2|$, $|S_4|$, $|S_3|$, $|S_5|$, $|S_2 + S_1 S_3|$, and $|S_4 + S_1 S_5|$. The coefficients $|S_3|$ and $|S_5|$ are known. The coefficients $|S_2|$, $|S_4|$, and $|S_2 + S_1 S_3|$ may be eliminated in favor of $|S_1|$. Then the above equation along with the physical Eq. (1.A10) is sufficient to specify the coefficients. We find that

$$\begin{aligned} |S_1|^2 &= |S_2|^2 = \frac{f_+}{f_-}(\mathrm{e}^{\eta_-} - 1) \\ |S_4|^2 &= 1 \\ |S_2 + S_1 S_3|^2 &= \frac{f_+}{f_-}\mathrm{e}^{-\eta_-}(1 - \mathrm{e}^{-\eta_-}) \\ |S_4 + S_1 S_5|^2 &= \mathrm{e}^{-2\eta_-} \end{aligned} \tag{1.A20}$$

The coefficients may be immediately determined from Eq. (1.A12)

$$C_{IC}^T = 1 - \mathrm{e}^{-\eta_-} \quad , \quad R_{IC} = \mathrm{e}^{-2\eta_-} \quad , \quad C_{IC}^R = \mathrm{e}^{-\eta_-}(1 - \mathrm{e}^{-\eta_-}) \tag{1.A21}$$

6 Appendix B: Equivalency of Coupling and Budden Tunneling for Large κ

The potential (1.69) is of the form

$$Q = \frac{c + dz}{f + gz} \tag{1.B1}$$

where

$$\begin{aligned} c &= \nu_{co}^2 - 1 - \kappa^2(\nu_{ii}^2 - 1) \\ d &= 2(\nu_{co}^2 - \nu_{ii}^2\kappa^2) \\ f &= 2(\nu_{ii}^2 - 1) \\ g &= 2((\nu_2^2 - 1)\kappa^2 + 2\nu_{ii}^2) \end{aligned} \tag{1.B2}$$

and

$$\nu_2 = \Omega_{c1}/\Omega_{c2}, \nu_{co} = \Omega_{c1}/\omega_{co}, \nu_{ii} = \Omega_{c1}/\omega_{ii} \tag{1.B3}$$

are various mass and density ratios. We recognize this potential to be a Budden equation with a cutoff and resonance. With the appropriate change of variables

$$x = -(f + gz) \tag{1.B4}$$

we recover the traditional form of the Budden equation (1.70) with

$$k_0^2 = d/g^3, \alpha = cg/d - f \tag{1.B5}$$

7 Appendix C: Relevant Frequencies in a Two-ion Species Plasma

Wave propagation in a cold, two-ion species plasma is characterized by the gyrofrequencies, $\Omega_{1,2}$, the cutoff frequency

$$\omega_{co} = (n_1\Omega_{c2} + n_2\Omega_{c1})/(n_1 + n_2) \tag{1.C1}$$

the crossover frequency

$$\omega_{cr}^2 = (n_1\Omega_{c2}^2 + n_2\Omega_{c1}^2)/(n_1 + n_2) \tag{1.C2}$$

and the ion-ion hybrid frequency

$$\omega_{ii} = \omega_{co}\frac{\Omega_{c1}\Omega_{c2}(n_1 + n_2)}{n_1\Omega_{c1} + n_2\Omega_{c2}} \tag{1.C3}$$

These frequencies have the well defined ordering

$$\Omega_{c1} < \omega_{ii} < \omega_{co} < \omega_{cr} < \Omega_{c2} \tag{1.C4}$$

Part 2
A Numerical Study of Mode Conversion

1 Introduction

In part 1 of this report we discussed the asymptotic behavior of low frequency modes which propagate at frequencies near the heavy ion gyrofrequency in a multispecies plasma. In that work it was our purpose to describe the behavior of waves which propagate from a region of low magnetic field into a region of large magnetic field. We found that the wave equations are amenable to a Wentzel-Kramers-Brillouin (WKB) analysis "far" from the crossover-cutoff-resonance triplet which occurs near the heavy ion gyrofrequency; however, there exists a regime within which such an analysis is inadequate, and the propagating modes couple strongly.

We characterized the behavior of various incident modes across this region by various transmission and absorption coefficients which corresponded to the Poynting flux attributable to each mode. From the value of these coefficients it is possible to infer the power apportioned to each mode given a wave incident in a particular mode. In addition, we found that substantial wave power is absorbed within this region. One physical interpretation of such absorption is that it provides a source for ion heating (perhaps through mode conversion to a thermal branch which can damp on the ions). In addition, the thermal population should also damp on the transmitted ion-cyclotron wave providing an additional source for heating.

In part 1 of this report we determined the primary transmission coefficient in all cases, and in the case of a large "gap," we determined the reflection coefficients as well. In a similar, but different, approach *Le Quéau and Roux* [1992] obtained the coefficients for the case of a small "gap" and quantified the associated absorption. For the case of large angle of propagation, we unambiguously determined the coefficients for the ion-cyclotron mode (the magnetosonic mode does not propagate in that regime). In all cases, the transmission is described by Budden-like transmission coefficients and a definite absorption characterized the transmission process.

In order to expand upon the results which we have obtained analytically and to unambiguously determine the wave power associated with each mode, we present a numerical solution to the differential equation associated with this problem. In particular, in the regime where the tunneling "gap" is small we obtain the exact solutions to the differential equation and from these extract the coefficients.

There are a number of advantages to be gained by considering a numerical solution. Within the context of a numerical solution, it is possible to retain the exact expressions for the Stix functions [*Stix*, 1962]. In order to obtain an analytical solution we linearized these functions. Within that approximation it is only possible to retain one ion resonance and one saddle point. However, as discussed in part 1, two saddle points exist at which coupling occurs. For small or large κ one or the other saddle point dominates the mode conversion process, but for intermediate κ both saddle points are important and the transition between them should be better understood. As we shall see, the presence of the extra terms does complicate the mode conversion process slightly. In addition, we shall see that at low altitudes the magnetosonic and ion-cyclotron branches couple strongly (this is the result of the coupling point at zero frequency described in the part 1) so that the transmitted wave amplitudes tend to be functions of altitude. Finally, we can model the variations in the magnetic field in a more realistic manner with a cubic dependence on altitude rather than a simple linear calculation.

In the remainder of this report, we develop and implement a reasonable procedure for extracting the values of the coefficients numerically. We then compare these numerical results with the analytical results presented in part 1 of this report.

2 Numerical Procedure

2.1 Basic Equations

In the analytic part we considered a specific problem in which waves propagate in the magnetosphere from a region of small magnetic field to a region of large magnetic field. As discussed in part 1, it is reasonable as a first approximation to consider wave propagation in a cold multispecies plasma. Furthermore, it is possible to reduce the problem to one dimension if we

consider variation only along the direction of the magnetic field. Such an approximation is reasonable in the specific context that we considered because parallel gradients are much larger than perpendicular gradients.

Given these approximations we derived a fourth-order coupled differential system which appropriately describes the electric field components perpendicular to the magnetic field

$$\epsilon^2 \Psi'' + \mathbf{M}\Psi = 0 \tag{2.1}$$

where

$$\mathbf{M} = \begin{pmatrix} r - \kappa^2/2 & \kappa^2/2 \\ \kappa^2/2 & l - \kappa^2/2 \end{pmatrix} \tag{2.2}$$

The two components of Ψ (ψ and ϕ) are the circularly polarized fields E_- and E_+ which are functions of the dimensionless coordinate, $z \equiv x/L_B$ where L_B is a conveniently chosen spatial scale. We have normalized the Stix functions, R and L, to the large ratio, c^2/v_{A0}^2 (v_{A0} is the Alfvén velocity at $\omega = \Omega_{c1}$), so that the functions

$$\begin{matrix} r \\ l \end{matrix} = \pm \frac{1}{g_A} \frac{\Omega_{c1}\Omega_{c2}}{\omega_{co}} \frac{(\omega \pm \omega_{co})}{(\omega \pm \Omega_{c1})(\omega \pm \Omega_{c2})} \tag{2.3}$$

are the order of unity. The function g_A contains the dependence of the Alfvén velocity on the coordinate, z; $\Omega_{1,2}$ are the heavy and light ion gyrofrequencies respectively; and $\omega_{co} = (n_1\Omega_{c2} + n_2\Omega_{c1})/(n_1 + n_2)$ is the cutoff frequency. The differential Eq. (2.1) is characterized by two other parameters: the small WKB parameter, $\epsilon \equiv 1/k_{A0}L_B$, and the normalized perpendicular wavevector, $\kappa \equiv k_\perp/k_{A0}$ where $k_{A0} \equiv \omega/v_{A0}$ is a typical wavevector.

In our approximation, the renormalized Stix functions (2.3) depend only on the magnetic field which we will define by the function

$$g(z) = \omega/\Omega_{c1}(z) \tag{2.4}$$

The particular form of the Stix functions

$$\begin{matrix} r \\ l \end{matrix} = \pm \frac{\nu_{co} \pm g}{(1 \pm g)(\nu_2 \pm g)} \frac{g}{g_A} \tag{2.5}$$

then only depends on the function g and the obvious mass and density ratios implied by the factors, ν, which are assumed to be constant. The function

g_A varies according to the Alfvén velocity along the field line ($Bn^{-1/2}$). For simplicity, we shall assume throughout the analysis that g_A remains constant (i.e. that the Alfvén velocity remains fixed). Such an assumption is certainly reasonable if the region of coupling is localized. In addition, such an assumption also allows us to match the WKB solutions more easily in the region of high field (low altitude). A more relevant manner in which to incorporate the actual decrease in the Alfvén velocity would be to incorporate mode solutions on the low altitude side of the resonance whose eigenvalues are determined by appropriate ionospheric boundary conditions [*Lysak and Dum*, 1983; *Lysak*, 1985]. Although perhaps slightly less realistic, our assumption, $g_A = 1$, should be sufficient to determine the coefficients to first order, and it is to be understood that inclusion of ionospheric boundary conditions is beyond the scope of the present work.

The function, g, contains all the essential information with regard to magnetic field variations. The most reasonable dependence for g on altitude is a dipole field. Thus, we expect that in physical coordinate, x, and scaled coordinate, z, the function, g, takes the form

$$g = \frac{L_B^3}{x^3} = \frac{1}{z^3} \tag{2.6}$$

where L_B is the factor which appears in ϵ. The proper choice for L_B in this instance is the altitude at which the wave frequency matches the gyrofrequency (the order of R_E).

Having thus relegated all functional dependence into the functions r and l through the function, g, we solve the differential Eq. (2.1) numerically. However, as discussed at length in part 1 of this report, the differential equation has a regular singular point at the location of the plasma resonance, namely where $z = 1$. For large values of z, $l > r$, and at the local crossover frequency $r = l$. The function l is characterized by a zero at the local cutoff frequency and a pole at the heavy ion resonance. The solution to Eq. (2.1) is multivalued and has a branch point at $z = 0$, so that in order to retain the appropriate physical behavior, we must continue the solution above the pole which may be physically interpreted as damping. Eq. (2.1) must therefore be suitably extended into the upper half of the complex plane so that the pole may be circumvented.

2.2 Numerical Technique

The technique that we use to solve Eq. (2.1) is in principle straightforward. Eq. (2.1) constitutes a system of eight fourth-order equations for the real and imaginary part of Ψ. One manner in which to continue the solution, Ψ, from the negative real axis to the positive real axis is to solve the differential equation along some parameterized path in the complex plane, $z(\tau)$, characterized by a real parameter τ. The solution is then obtained by solving the equivalent eight first-order ODE's in the parameter τ by means of a well known integrating scheme such as the Runge-Kutta, Bulirsch-Stoer, or the predictor-corrector method [*Press et al.*, 1986]. The generalization of Eq. (2.1) to a continuous (although not necessarily smooth) path is straightforward and is discussed in detail elsewhere [*Johnson*, 1992].

In order to obtain the correct branch of the multivalued solution of Eq. (2.1) we must continue the solution above the pole at $z = 0$ in the complex plane. Therefore, we solve the differential equation along a parameterized path which passes above the pole. Suppose that we know the solution, Ψ, at some point, z_0, along the negative real axis. In order to determine the value of the solution at some point, z, along the real axis, we may integrate the equivalent differential equation along the parameterized path such as that illustrated in Figure 7.

$$\begin{array}{ll} z_1(\tau) = \tau & z_0 < \tau < 1-\rho \\ z_2(\tau) = \rho \exp\left(i\frac{\pi}{2}(1+\frac{1-\tau}{\rho})\right) & 1-\rho < \tau < 1+\rho \\ z_3(\tau) = \tau & 1+\rho < \tau < z \end{array} \qquad (2.7)$$

which consists of integration along the real axis from z_0 to $1-\rho$ (recall that the pole is at $z = 1$) followed by integration along a circular arc above the pole to $1+\rho$ on the real axis. Finally, the solution at z may be obtained from further integration along the real axis. The solution must not depend on the choice of ρ or for that matter upon the choice of parameterized path. This requirement provides an additional check on the reliability of the procedure.

A general solution to the differential equation may be obtained by taking four different initial conditions at the point z_0 which correspond to four linearly independent solutions. Once we have found a general solution to the differential equation we may decompose it into its constituent WKB solutions. Far from the coupling region, the WKB solutions are asymptotically

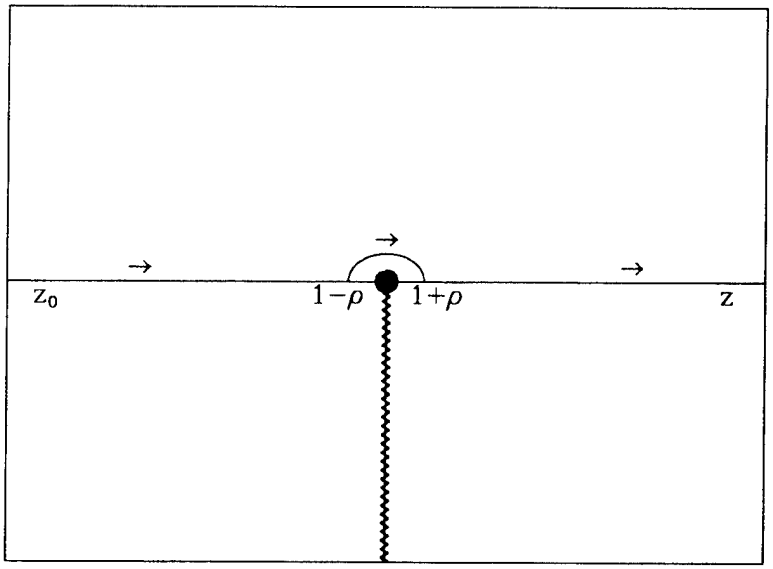

Figure 7: The parameterized path along which we solve the differential equation consists of three contours. The first integrates along the real axis to some point ρ. To continue the solution to the positive real axis, we take a contour along a circular arc above the pole. Finally the solution may be obtained by continuing the solution along the real axis.

close (in the parameter ϵ) to the actual solutions.

2.3 Extracting the Coefficients

Once four linearly independent solutions for the lower component, ψ, of Ψ have been calculated (ψ_j, $j = 1, 4$) using the method detailed in the last section, it is relatively straightforward to determine the coefficients. In the asymptotic regime, the WKB analysis yields four solutions (Θ_j, $j = 1, 4$). In the asymptotic region far to the left of the coupling region along the negative real axis and far to the right along the positive real axis the WKB solutions are reasonable approximations to the actual solutions and serve as basis functions as illustrated in Figure 8.

The general solution to the upper component of (2.1) may be written in

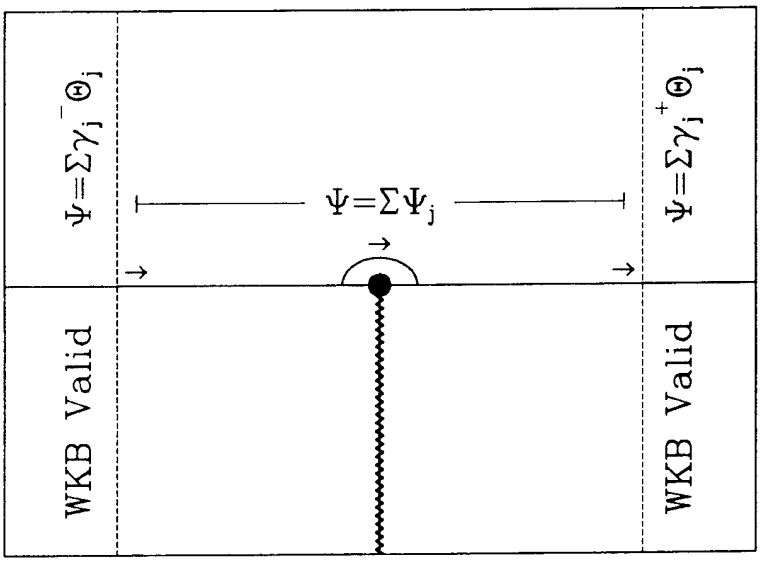

Figure 8: In regions far from the pole the WKB solutions are asymptotically valid. The numerical solution connects the regions in which the WKB solutions are accurate.

the form

$$\psi = \alpha_j \psi_j \tag{2.8}$$

where we have introduced the summation notation. Four appropriate boundary conditions are sufficient to determine a particular solution of the differential equation. The boundary conditions which we impose on the solution are related to the coefficients of the WKB solutions above and below the coupling region. Because the WKB solutions are basis functions in the asymptotic regime, the solution, ψ, may be decomposed as

$$\psi = \gamma_j^{\pm} \Theta_j \quad , \quad \Re(z) \to \pm\infty \tag{2.9}$$

where the decomposition may be different along the positive and negative real axis in light of the Stokes phenomenon [*Heading*, 1962]. In the following analysis we will refer to the region $\Re(z) \to +\infty$ as "above" (low field side) and we will describe waves propagating from $\Re(z) > 0$ to $\Re(z) < 0$ as "downgoing" waves ("below" and "upgoing" have the obvious meanings).

The boundary conditions are related to the power flow through the conserved quantity

$$\mathcal{J} = i(\Psi^{\dagger\prime}\Psi - \Psi^{\dagger}\Psi') \tag{2.10}$$

i.e., the field aligned Poynting flux, described in part 1. As detailed in Appendix A, the coefficients, γ, correspond to power flux in the four propagating modes. To clearly specify the boundary conditions we choose Θ_j as specified in Appendix A corresponding for parallel propagation to a downgoing left-hand circularly polarized (LHCP) wave, upgoing LHCP wave, downgoing right-hand circularly polarized (RHCP) wave, and an upgoing RHCP wave respectively.

The values of $\gamma^{\pm}$ must be consistent with the boundary conditions related to our problem. For a downgoing magnetosonic wave we require that

$$\gamma^{+} = \begin{pmatrix} 0 \\ c_2 \\ 1 \\ c_4 \end{pmatrix} , \begin{pmatrix} c_1 \\ 0 \\ c_3 \\ 0 \end{pmatrix} \tag{2.11}$$

Physically, these conditions correspond to no upgoing waves from below the coupling region, and above the coupling region, the only incident wave is the downcoming approximately RHCP mode. The amplitudes, c_j, are to be determined and are related to the power transmitted in the incident mode, T_{MS} (c_3); reflected in the incident mode, R_{MS} (c_4); transmitted in the coupled mode, C^R_{MS} (c_2); and reflected in the coupled mode, C^T_{MS} (c_1).

For an incident ion-cyclotron wave, we require that the amplitudes, $\gamma^{\pm}$, take the form

$$\gamma^{+} = \begin{pmatrix} 1 \\ c_2' \\ 0 \\ c_4' \end{pmatrix} , \begin{pmatrix} c_1' \\ 0 \\ c_3' \\ 0 \end{pmatrix} \tag{2.12}$$

consonant with the physical boundary conditions. In this case c_j' correspond to transmitted, T_{IC}; reflected, R_{IC}; coupled transmitted, C^T_{IC}; and coupled reflected, C^R_{IC}, wave power respectively.

In order to determine the coefficients, α_j, we decompose the linearly independent functions, ψ_j, into the constituent WKB solutions on both the positive and negative imaginary axis. In light of the Stokes phenomena, the

expansions are not the same. Then

$$\psi_j = \mu_{jk}^{\pm}\Theta_k \quad , \quad \Re(z) \to \pm\infty \tag{2.13}$$

which determines the relationship between the coefficients

$$\gamma_l^{\pm} = \alpha_j \mu_{jl}^{\pm} \tag{2.14}$$

The Eq. (2.14) constitute a system of 8 complex equations in 8 unknown complex variables. The variables which must be determined are the values of α_j and the amplitudes, c_j or c_j'. The values of α are obtained from the four equations with definite boundary conditions. The values of the amplitudes are determined by the remaining four equations. The amplitudes determine the power flow and, thus, the coefficients T, R C^T, and C^R as detailed in Appendix A. In either the case of incident magnetosonic or ion cyclotron waves, the absorption coefficient is of the form

$$A \equiv 1 - (T + R + C^R + C^T) \tag{2.15}$$

The physical interpretation of the coefficients is discussed in Figures 1.3 and 1.4.

3 Numerical Complications

In studying the ideal system of Eq. (2.1) with the well approximated spatial dependence on the magnetic field, it is important for us to address some basic limitations in the numerical analysis. Numerically, the equations are sufficiently tractable that the exact solution to the well approximated Eq. (2.1) may be determined to arbitrary accuracy (within the limits of computer accuracy). We can make a statement such as this for a number of reasons. We have solved the differential equation using three different techniques, Bulirsh-Stoer, Runge-Kutta and predictor-corrector [*Press et al.*, 1986]. All techniques produce the same results to within the limitations of double precision accuracy. Moreover, we have transformed the Eq. (2.1), using a Ricatti Transform, into a set of first-order non-linear differential equations [*Smith and Whitson*, 1978]. (Such a transformation is particularly useful for suppressing exponentially growing solutions.) The numerical solution that we have obtained to the transformed Ricatti equation is again consistent with

the numerical solution of (2.1) to arbitrary accuracy. In principle, then, the accuracy of the coefficients that we determine is limited to the accuracy of the imposed boundary conditions.

The boundary conditions which we impose upon the numerical solution are at best limited to the validity of the WKB solutions. That is, the accuracy of the coefficients is limited by the accuracy of $\mu_{jk}^{\pm}$. Once a numerical solution ψ_j is obtained, the most straightforward manner in which to determine the coefficients, $\mu_{jk}^{\pm}$, is to compare the value of the numerical solution, ψ_j, with the four WKB solutions, Θ_j, at four different locations. Alternatively, we could match ψ_j and its derivatives at a single point with the Θ_j and their derivatives. More elaborate schemes are also conceivable in which ψ_j is matched in a number of locations and an average taken. Moreover, because we consider only the leading order WKB approximation, it is important that we match the numerical and WKB solutions in a region small compared to a typical wavelength. On the other hand, if this region is taken too small, then the values of Θ_j do not vary sufficiently to determine the coefficients $\mu_{jk}^{\pm}$ to the required accuracy. Indeed, the quality of the matching is a basic limitation of our analysis. In the results which follow, we have matched the solutions in a region such that the WKB approximation is reasonably valid, and we have varied the width of the matching region and found that within the upper and lower limits mentioned above deviations from the presented results are not substantial.

For large values of κ, the RHCP magnetosonic mode has very small n_- so that matching to the WKB solutions becomes somewhat suspect. One should therefore question the exact manner in which the coefficients behave near the critical κ, which corresponds to the transition from four propagating WKB modes to two propagating modes, because the meaning of matching to WKB boundary conditions is questionable. However, we should point out that the coefficients do behave reasonably smoothly and it is not unreasonable to assume that the asymptotic solutions are reasonably accurate even when the WKB smallness parameter, $\epsilon \sim 1$ [*Bender and Orszag*, 1978].

We should also mention the dependence of the solutions on the parameter, ρ, which was introduced to circumvent the pole at $z = 1$. The solutions ψ_j have virtually no dependence on the parameter ρ as long as ρ is taken sufficiently small. In the case of very large ρ, the exponentially growing solution in the upper half plane dominates the subdominant solution to the machine precision in which case an inaccurate numerical solution is obtained.

For all results presented, the value of ρ is taken sufficiently small so that numerical stability is retained.

Finally, as $z \to 0$ so that $g \to \infty$ we find that $r = l$ which corresponds to the lower crossover frequency. Coupling associated with this crossover frequency occurs between $z = 0$ and $z = 1$. Moreover, the strong dependence of the magnetic field on z^{-3} means that this coupling occurs over an extended range of z ($r \approx l$ over a large range). As a result, the numerical values of the coupling coefficients are functions of altitude. However, the physical boundary conditions which we impose on the upgoing waves below the heavy ion resonance are independent of the location at which we match the solutions. Then it turns out that the reflection and absorption coefficients do not depend upon the location at which the solution is matched for $z < 1$; however, the relative value of the transmission coefficients will depend upon the location at which they are evaluated to a slight degree because the two downgoing Alfvén modes couple at low altitudes. In the following analysis we match to the slowly varying WKB solutions at some point between $z = 0$ and $z = 1$. In all cases, we have chosen to evaluate the coefficients in a range over which the variation of the coupling coefficients with altitude is small. Indeed, this range is identically the altitude range over which the boundary conditions may be optimally described in terms of the coefficients of the WKB solutions.

4 Results

4.1 Parameter Regime

In the following sections we determine the coefficients for several cases of incidence as described previously. The parameters which are of greatest interest are the magnetic field, magnetic field scale length, and the masses and densities of the various constituent ions. The masses are fixed parameters which we take to be hydrogen and oxygen (both singly ionized). The magnetic field and densities are embedded in the WKB parameter ϵ and the functions r and l depend only upon the density ratios. Hence, a particular solution is determined from the specification of ϵ and the concentration of the minority

species η. Typical values for the parameter ϵ are

$$\epsilon = \frac{1}{k_A L_B} \approx 0.5 r^{-1} \rho^{-1} \tag{2.16}$$

where r is the scale length in earth radii ($\sim 1 - 3$) and ρ is the mass density of ions ($\sim 1 - 100$) [*Moore et al.*, 1987, and references therein]. We will explore the parameter space for ϵ ranging from approximately 0.2 to 0.03. In this range, the WKB approximation is good and should provide reasonable matching conditions to the WKB solutions. We will in all cases concentrate on that range of oxygen concentration consistent with reasonable absorption levels. We have found this range to vary from 0.5 to 5 percent. In order to consider the limiting case of a large "gap" we will take ϵ to be small and η to be large.

4.2 Incident Magnetosonic Waves

For the results of this section, we impose the boundary conditions for downcoming magnetosonic waves and obtain the coefficients (2.A7). At this juncture it would be useful for the reader to examine Figure 3 to understand the physical meaning of the coefficients. In that figure a wave is incident on the magnetosonic branch with unit flux. The fractions of wave flux T_{MS} and R_{MS} are transmitted and reflected on the magnetosonic branch while the fractions C^R_{MS} and C^T_{MS} are transmitted and reflected along the ion-cyclotron branches as indicated.

We have obtained full analytical solutions for the limit of a large "gap." In Figure 9, we show the numerical solutions to the differential equation. Superimposed on the graph we have shown the analytical results (1.44) which we have obtained from a phase integral analysis consistent with a large "gap" for which there is no absorption. The results are in very good agreement. The most striking difference is that the coefficient C^T_{MS} is non-zero in contrast to the analytic situation. However, the analytical results only incorporate the existence of the coupling point near the crossover frequency. As discussed in part 1, coupling between the two Alfvén waves can be very strong at frequencies below the heavy ion-cyclotron frequency. It is this coupling which gives rise to the wave power found on the ion cyclotron branch.

In Figure 10, we compare the numerical transmission coefficient for a

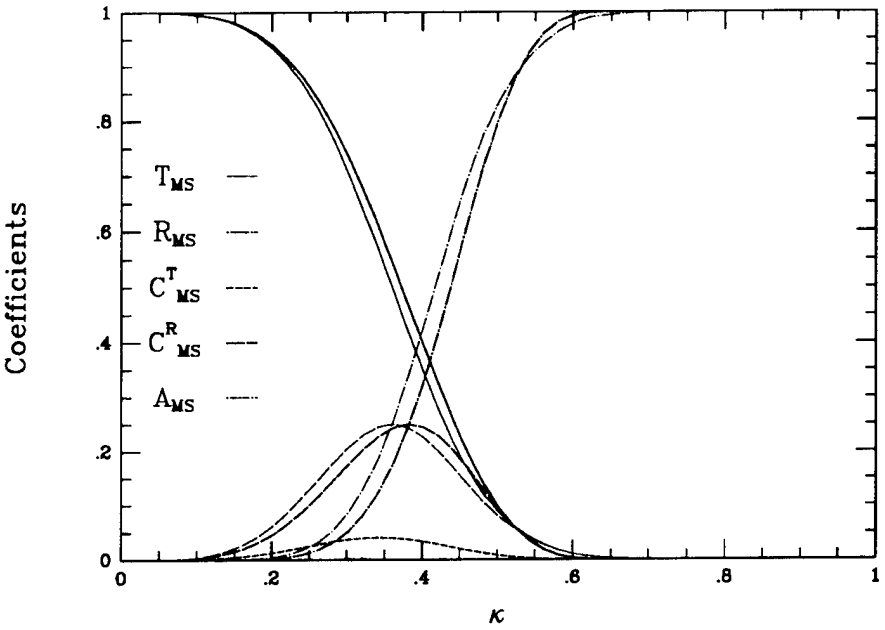

Figure 9: For the limit of large "gap" the numerical solutions and the analytical results are in reasonable agreement. We have taken ϵ=0.03 and $\eta = 5\%$ for which there is no absorption. The numerical solutions are plotted in heavy set type and the analytical results are indicated in light type. Note that for the numerical results the coefficient $\exp(-\pi\beta_+/\epsilon)$ although small is nonzero in contrast to the analytical results. This behavior is the result of coupling between the two Alfvén waves below the ion resonance corresponding to the coupling point at zero frequency.

small "gap" with the analytical result (1.44). We have plotted the numerical transmission coefficient in heavy solid and the analytical coefficient in light solid. The analytical results predict no coupled wave C^T_{MS}. However, coupling between the two modes does occur below the heavy ion resonance. Because this coupling does not involve reflection one might expect the total transmission $T_{MS}+C^T_{MS}$ to match the analytical transmission coefficient. We have plotted this sum as a dashed line. Indeed the sum compares well with the analytical results.

In the regime which corresponds to a large "gap" our numerical results are in good agreement with the analytical results. Moreover, even in the limit of a small "gap," the analytical results are in reasonable agreement. Let us now

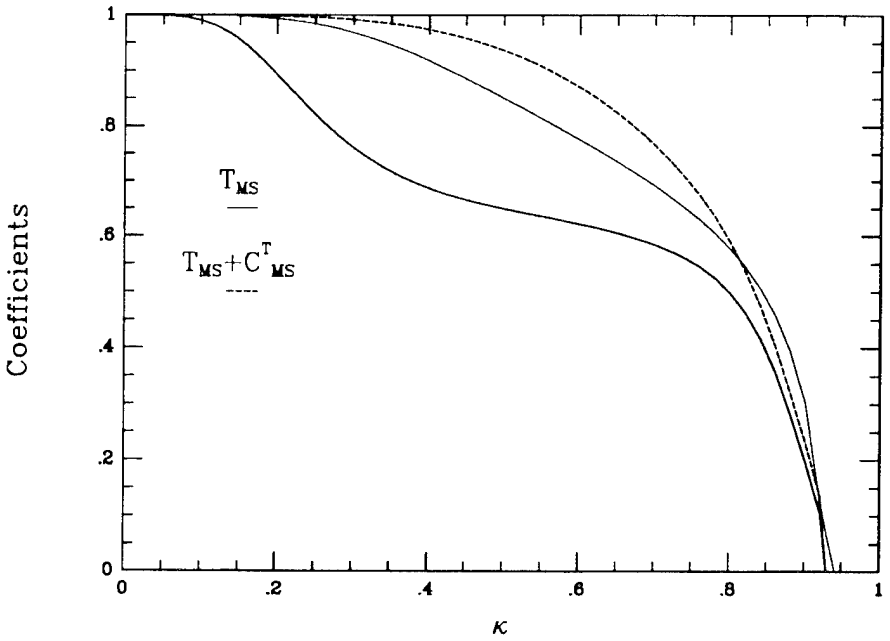

Figure 10: Transmission coefficient for the magnetosonic wave in the limit of small "gap" with ϵ=0.2 and $\eta = 1\%$. Note that the total transmission is in good agreement with analytical result.

explore the parameter space. In Figure 11 we have plotted the coefficients for the case $\epsilon = 0.2$ and $\eta = 1\%$. For parallel propagation, no coupling occurs. As the κ increases strong coupling between the two transmitted Alfvén waves occurs, and the sum of of those coefficients reproduces the analytical transmission coefficient. For large κ waves are reflected in the two upward propagating modes. The cutoff frequency increases substantially for large enough κ and the "gap" becomes too large to penetrate. In this case the reflection coefficient grows rapidly, and for $\kappa \approx 0.95$ the magnetosonic wave no longer propagates (the wave is reflected at the lower hybrid frequency well above the hydrogen gyrofrequency). For a substantial range of κ strong absorption occurs peaking at 20% for large κ.

For smaller densities, the absorption increases to about 25% although it tends to sharpen and occur mostly at large κ. Indeed, as the minority species density tends to zero, the transmission coefficient, T_{MS}, is approximately 1 and all other coefficients vanish. This means, in effect, that for very small oxygen densities the waves propagate as if there were no oxygen present.

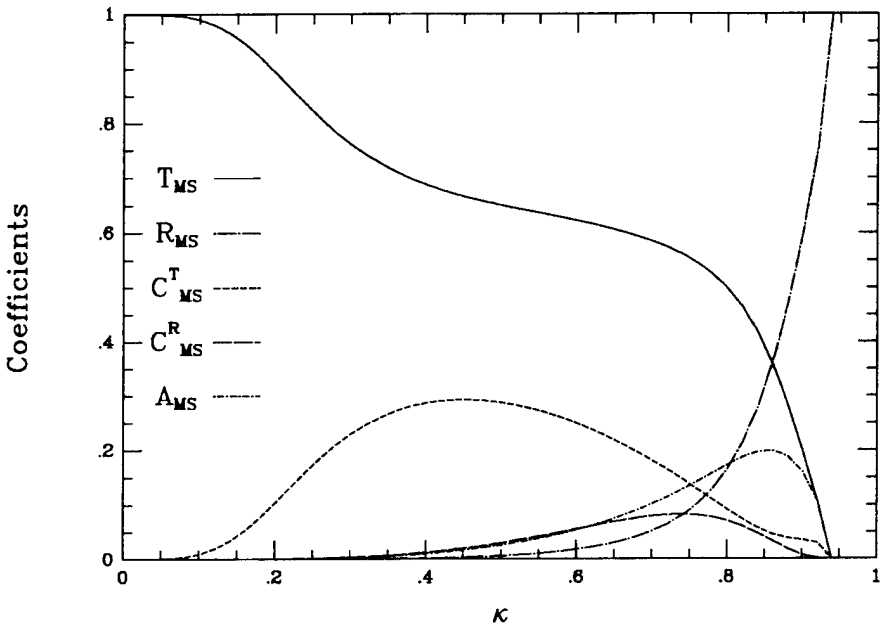

Figure 11: Coefficients for the case $\epsilon = 0.2$ and $\eta = 1\%$.

For larger densities ($\eta = 5\%$), as illustrated in Figure 12, we find that the absorption diminishes rapidly although the waves still couple at low altitude. In addition, we find that total reflection occurs at a much smaller value for κ. Absorption appears to be very small. However, one should keep in mind that in the case of a large gap all power upcoming in the LHCP mode will be absorbed. If perfect reflection were to occur at ionospheric altitudes, it is conceivable that a substantial portion of C^T_{MS} would also be absorbed.

For smaller values of ϵ (=0.08), as illustrated in Figure 13, we find that less coupling occurs between the two downgoing transmitted waves. In addition, reflection is much stronger at intermediate values of κ. This is because the "gap" contains more wavelengths and transmission is substantially diminished. Reasonably strong absorption still occurs over a vast range of κ and is typically about 7 percent. It should also be noted that a substantial portion of the reflected wave C^T_{MS} can also contribute to heating upon reflection. For even smaller values of the parameter ϵ (=0.03) we find that the absorption becomes negligible for $\eta > 1\%$, however, the absorption remains reasonably significant for $\eta = 0.5\%$.

In summary, we have found that incident magnetosonic waves couple

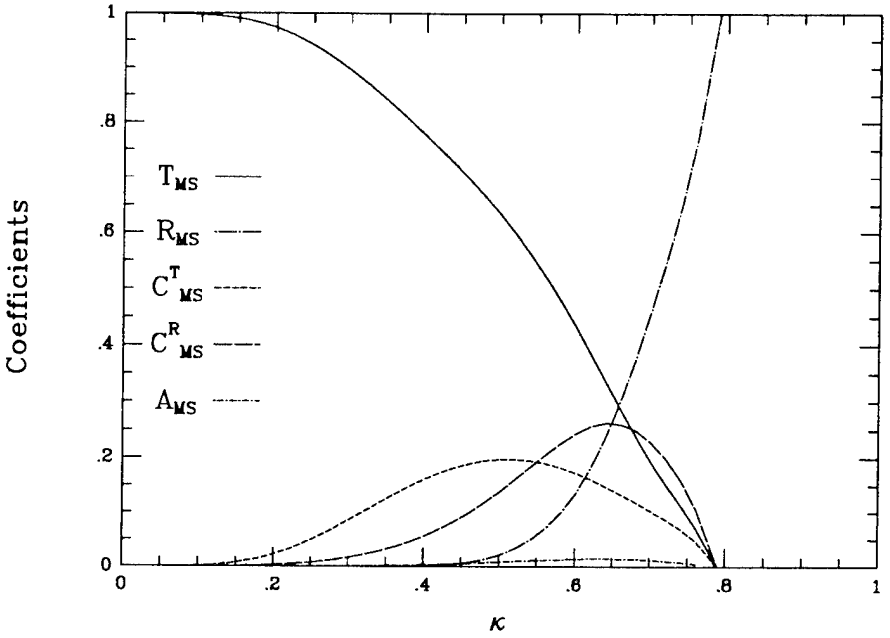

Figure 12: Coefficients for the case $\epsilon = 0.2$ and $\eta = 5\%$.

strongly near the crossover frequency for reasonable values of the minority species density. For larger values of κ the waves are completely reflected, and strong absorption occurs over a substantial range of κ.

4.3 Incident Ion-Cyclotron Waves

For the results of this section, we impose the boundary conditions for downcoming magnetosonic waves and obtain the coefficients (2.A8). For values of κ smaller than the critical κ for which the magnetosonic mode is cut off we determine these values numerically. For larger values of κ we use the analytical results obtained in part 1. Numerical extraction of the coefficients in the case of large κ involves substantial complications. In this section we will obtain correct estimates of the absorption for both small and large values of κ, and we will discuss the meaning and correctness of evaluating the coefficients for intermediate κ.

First, let us consider the coefficients for values of κ smaller than the critical κ for which the magnetosonic mode is cut-off. In order to understand the meaning of these coefficients is illustrated in Figure 4. A wave is incident on

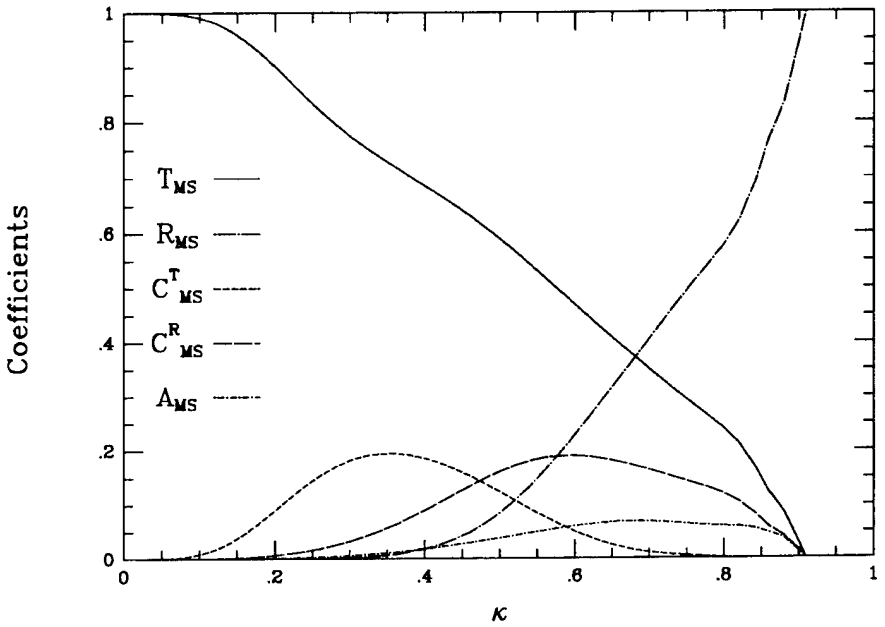

Figure 13: Coefficients for the case ϵ=0.08 and $\eta = 1\%$.

the ion-cyclotron branch with unit flux. The fractions of wave flux T_{IC} and R_{IC} are transmitted and reflected on the ion-cyclotron branches while the fractions C^R_{IC} and C^T_{IC} are transmitted and reflected along the magnetosonic branch as indicated.

We have obtained full analytical solutions for the limit of a large "gap." In Figure 14 we show the numerical solutions to the differential equation. Superimposed on the graph we have shown the analytical results (1.43) which we have obtained from a phase integral analysis consistent with a large "gap" for which there is no absorption. As for the case of an incident magnetosonic wave, the results are in very good agreement. Again a small amount of wave flux is found in the coupled transmitted wave.

In Figure 15 we compare the analytic solution for a small "gap" with the numerical calculation. Once again coupling between the two transmitted modes diminishes the power found on the transmitted ion-cyclotron mode. However, the results are certainly quantitatively correct for small values of κ in which case the low frequency coupling point does not enter into the calculation. For larger κ, the results are qualitatively correct and are good for an order of magnitude estimate; however, the existence of two **different**

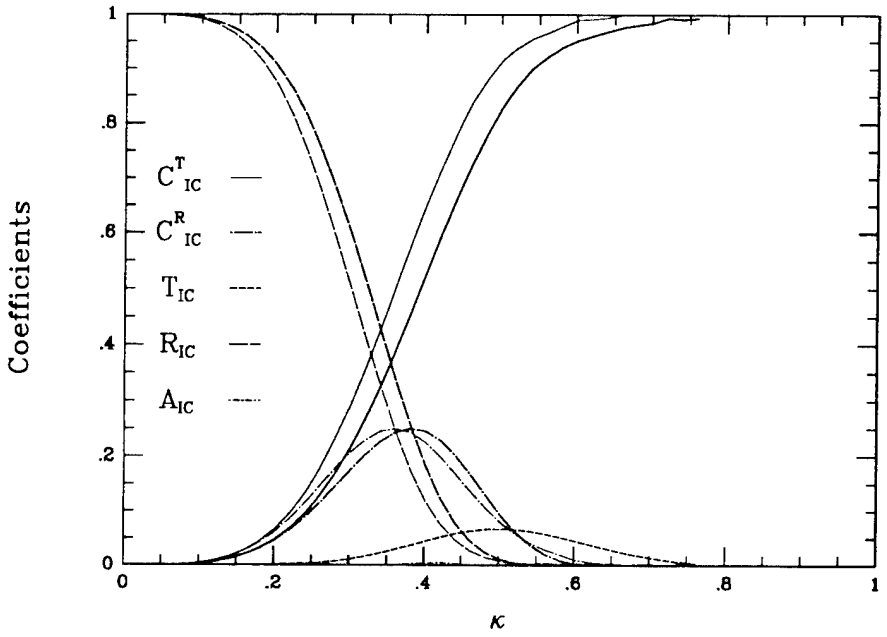

Figure 14: For the limit of large "gap" the numerical solutions and the analytical results are in reasonable agreement. We have taken $\epsilon = 0.03$ and $\eta = 5\%$ for which there is no absorption. The numerical solutions are plotted in heavy set type and the analytical results are indicated in light type.

coupling points (low frequency and crossover—see Figure 2) cannot be incorporated into a linear model and the analytic results are most accurate when the coupling is dominated by one of the two coupling points.

In Figure 16 we have plotted the coefficients for the case $\epsilon = 0.2$ and $\eta = 1\%$. For parallel propagation, the problem is described as a Budden tunneling problem for the ion-cyclotron branch, and the ion-cyclotron and magnetosonic branches do not couple. For larger angles of propagation, the tunneling increases as, in fact, predicted by the analytical analysis in Figure 15. For larger values of κ, coupling between the downgoing modes occurs at the crossover frequency, and substantial wave energy is transferred to the coupled magnetosonic wave. Indeed, for the case of a small "gap" as in Figure 14, coupling to the coupled transmitted wave, C^T_{IC}, is complete for large values of κ. Substantial absorption occurs over a very large range of κ taking a value over 20% over most of the range. In Figure 17 we explore the transmission coefficients for parallel propagation for $\epsilon = 0.2$ (for parallel

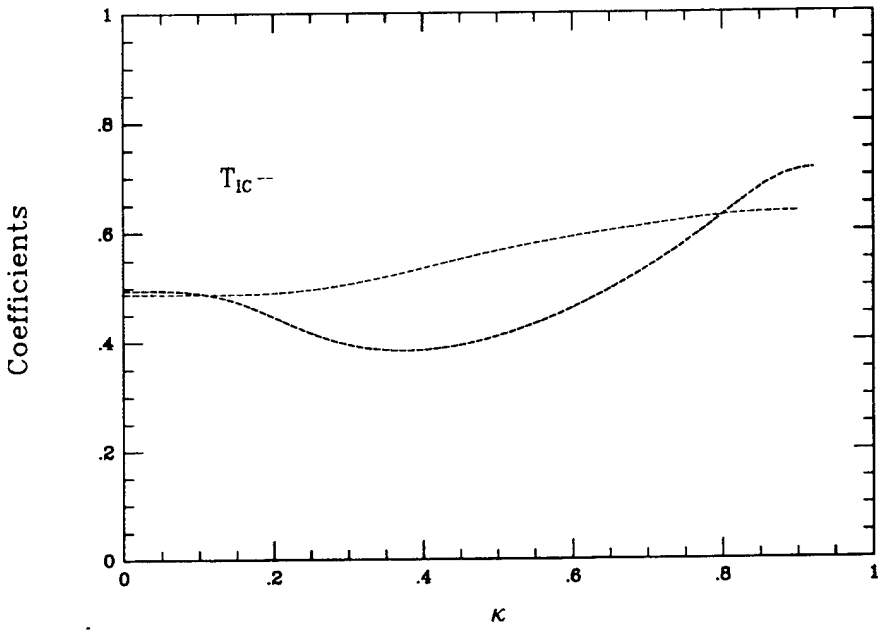

Figure 15: Transmission coefficient for the ion-cyclotron wave in the limit of small "gap" with $\epsilon = 0.2$ and $\eta = 5\%$. Note that the transmission is in best agreement for small κ.

propagation the two modes are uncoupled so that $C_{IC}^R = C_{IC}^T = 0$). As is clear, substantial absorption occurs over a large range of densities ranging from $\eta = 0.5\%$ to $\eta = 4\%$. For larger values of κ, the absorption remains essentially the same as for parallel propagation up to reasonably large values of κ.

As for the magnetosonic case, substantial absorption still occurs for $\epsilon = 0.08$ as indicated in Figure 18. In this case, the "gap" is large so that most of the wave power is reflected at small angles of propagation rather than transmitted; however, for larger angles of propagation, tunneling in both modes increases substantially until most of the power is coupled into the magnetosonic branch. For the case of parallel propagation with $\epsilon = 0.08$, the peak absorption levels are skewed toward smaller values of density ($\eta = 0.5\%$). For smaller values of ϵ the absorption is completely negligible and the wave is completely reflected.

For large values of κ, we have shown using a variety of methods that the transmission properties are described as a Budden tunneling problem

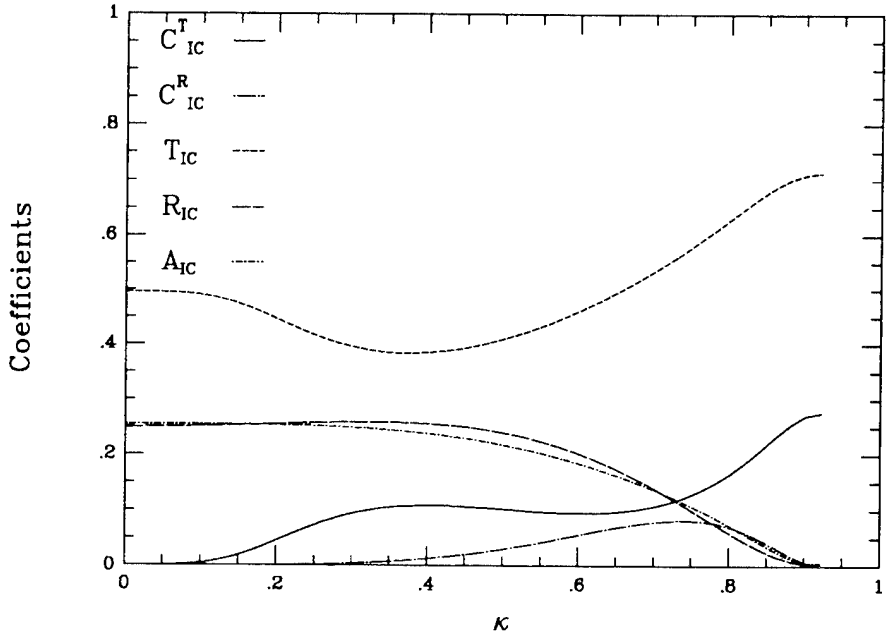

Figure 16: Coefficients for the case $\epsilon = 0.2$ and $\eta = 1\%$.

at the ion-ion hybrid frequency. Let us consider the analytical results. In Figure 19 we have plotted in bold type the transmission factors found in Eq. (1.54, 1.58) along with the corresponding absorption factor. Physically, the coefficients correspond to Figure 6. In light type we have plotted the transmission factors obtained from the embedded Eq. (1.71). They are in good agreement in the regime in which they are both valid. It is to be noted that there is reasonable agreement between the transmission factor, T_{IC}, near the upper bound of the numerical solution of Figure 16 and the large κ solutions of Figure 19. The absorption and reflection coefficients do not match well. While it is to be expected that the dominant WKB solution would be continuous in κ it is not necessarily expected that the coefficient of the subdominant solutions would remain continuous.

For large κ the transmission coefficients approach a constant value determined from Budden tunneling at the ion-ion hybrid frequency. In Figure 20 we plot the coefficients against the concentration of oxygen. As for the case of parallel propagation strong absorption occurs for a large range of densities ranging from $\eta = 0.5\%$ to $\eta = 7\%$. In all cases the absorption remains essentially constant for $\kappa > 1$.

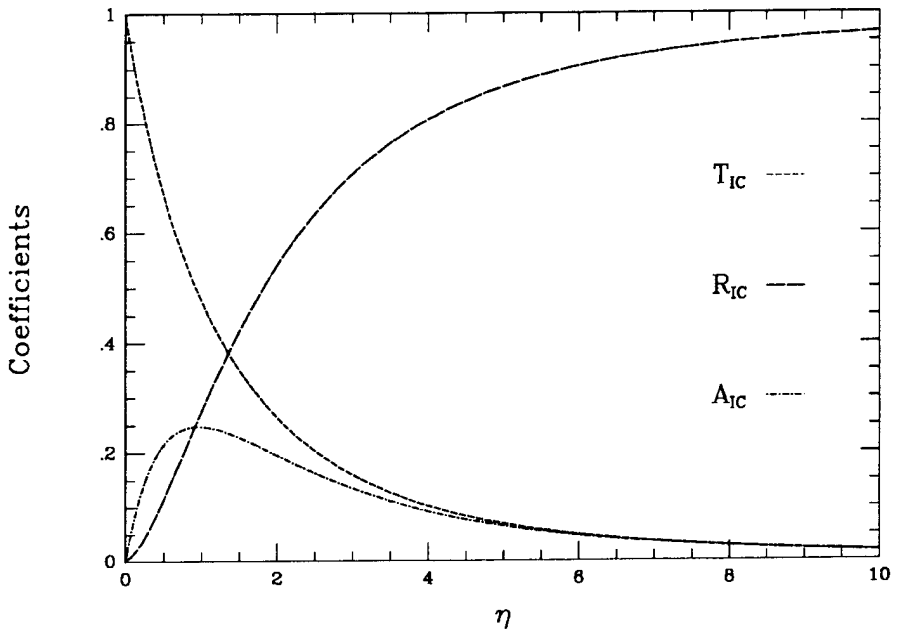

Figure 17: Coefficients for parallel propagation with $\epsilon = 0.2$. Strong absorption occurs for $0.5\% < \eta < 4\%$.

For smaller values of ϵ the absorption still remains very large for reasonable densities. As illustrated in Figure 21 although the reflection is now much larger than the transmission, the absorption remains over 20factor, T_{IC}, again matches reasonably well with that coefficient for small κ (see Figure 18), but the other coefficients are again discontinuous. From Figure 22, it is clear why the transmission has not diminished from the case with $\epsilon = 0.2$. The absorption is strongly peaked around $\eta = 1$. For smaller values of ϵ the region of strong absorption moves to very small (probably unphysical) values of η.

In summary, we have found that incident ion-cyclotron waves undergo Budden-like tunneling at the cutoff frequency for nearly parallel propagation and at the ion-ion hybrid frequency for nearly perpendicular propagation. The absorption is very strong over a large range of κ and for a reasonable range of *eta*. For intermediate values of κ, coupling near the crossover frequency becomes important and a substantial amount of wave power is transmitted in the magnetosonic mode. However, for large enough κ, the magnetosonic mode is cut-off and that wave power is reflected back into the

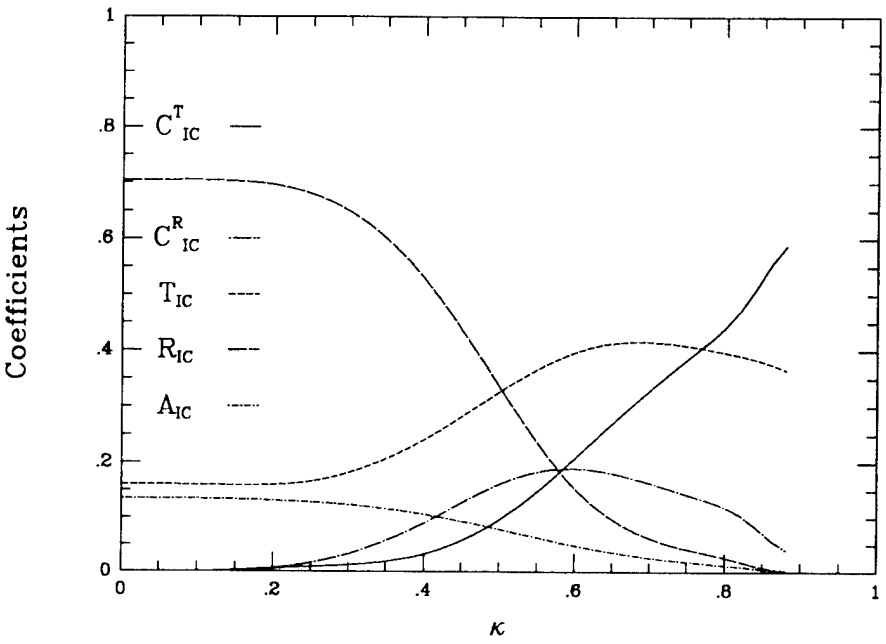

Figure 18: Coefficients for the case $\epsilon = 0.08$ and $\eta = 1\%$.

system.

4.4 Validity of Analytic Approximation

The analytic results that were obtained in part 1 and those obtained by *Le Quéau and Roux* [1992] are in excellent agreement for small and large κ for which one or the other of the two saddle points dominate the mode conversion process. However, for a small "gap" there is substantial coupling between the two downgoing modes resulting from the cutoff saddle point. The numerical results have the advantage of being able to retain both saddle points. It is also important to point out that the absorptions published by *Le Quéau and Roux* [1992] are somewhat misleading. They show strong absorption for $\eta \approx 10 - 50\%$. First, their approximation is only valid for densities less than 3%. Secondly, our results clearly show that absorption is at best limited to densities below about 5%. The reason behind this discrepancy is that they have fixed the ratio their tunneling factor, $\eta L_B/\lambda$, so that the WKB approximation is actually not valid for η more than about 1%.

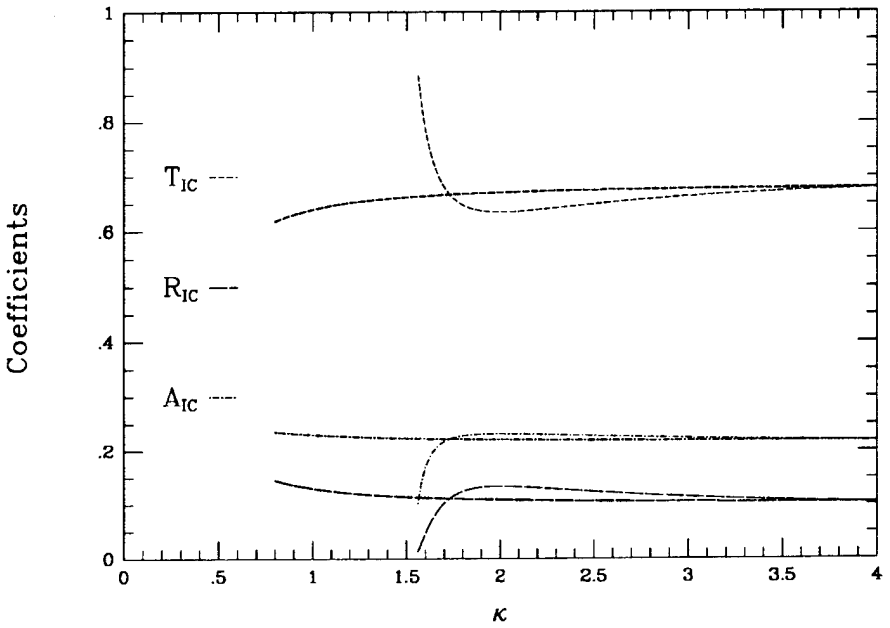

Figure 19: Analytical approximations for the transmission coefficients for $\epsilon = 0.2$ and $\eta = 1\%$ at large κ (which corresponds to large angles of propagation). We have plotted the coefficients related to the phase integral transmission, $\exp(-\pi\beta_+/\epsilon)$, in dark type. The transmission coefficients found from the embedded Budden equation for tunneling through the "gap" are indicated in light type.

4.5 Physical Considerations

We have found that the analysis of an incident ion-cyclotron wave is somewhat more complicated than the magnetosonic case in that it involves an interesting change in the behavior for the coefficients for small and large κ. In particular, it is important to realize that the continuity of the the transmission properties for these waves is somewhat dependent upon the model from which boundary conditions are obtained. The fact that two different regimes exist for $\kappa < 1$ and $\kappa > 1$ is represented by the transition of the cutoff frequency where a cutoff appears below the ion-cyclotron frequency (instead of above). Then the boundary conditions at $\pm\infty$ are determined by two WKB solutions rather than four. One expects that such a sudden transition in the behavior of the modes is not physically meaningful although it

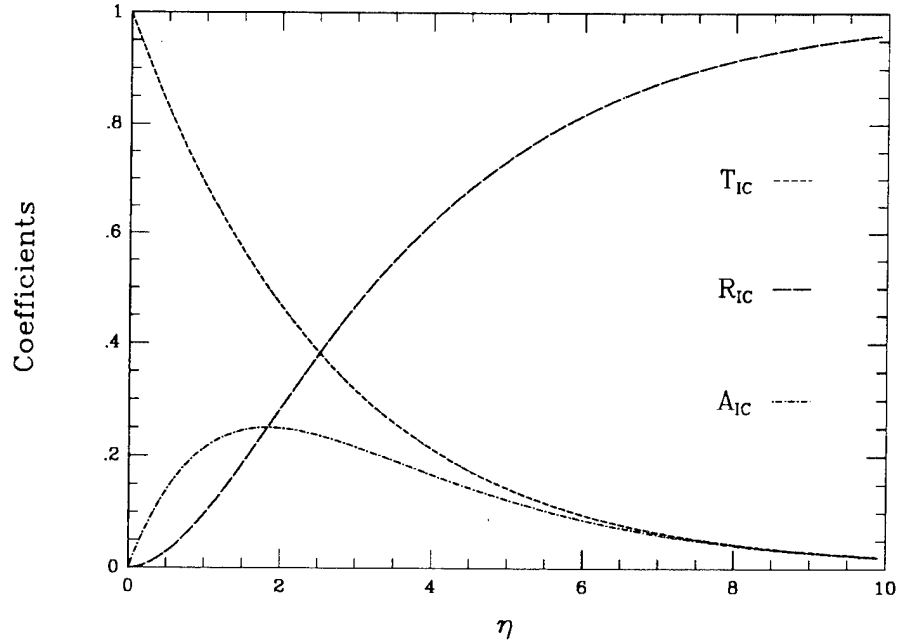

Figure 20: Coefficients for large κ with $\epsilon = 0.2$. Strong absorption occurs for $0.5\% < \eta < 5\%$.

is certainly mathematically feasible (recall the discussion of the sudden jump in the Stokes coefficients across a definite value for $Arg(z)$).

In light of our present model, simply from physical considerations we would expect to find a discontinuous jump in the absorption coefficient as the cutoff moves from $+\infty$ to $-\infty$. If the magnetosonic mode propagates at $-\infty$ then one expects to find that all the wave power on the magnetosonic mode is transmitted; however, if that mode is reflected above the region where the coefficients are evaluated, then all of the wave power, C_{IC}^T, on that branch is reflected back into the system. Because C_{IC}^T increases substantially at large κ where coupling at the crossover frequency is most complete, this amount of reflected energy is substantial. Such reflection greatly modifies the reflection and absorption coefficients although it should not affect the transmission coefficient. As we have seen, the transmission coefficient actually matches reasonably well across the critical κ.

Physically, we might expect more continuous behavior for the coefficients; however, producing a more continuous result does not mean either solving the present equations more accurately or approximating the governing equa-

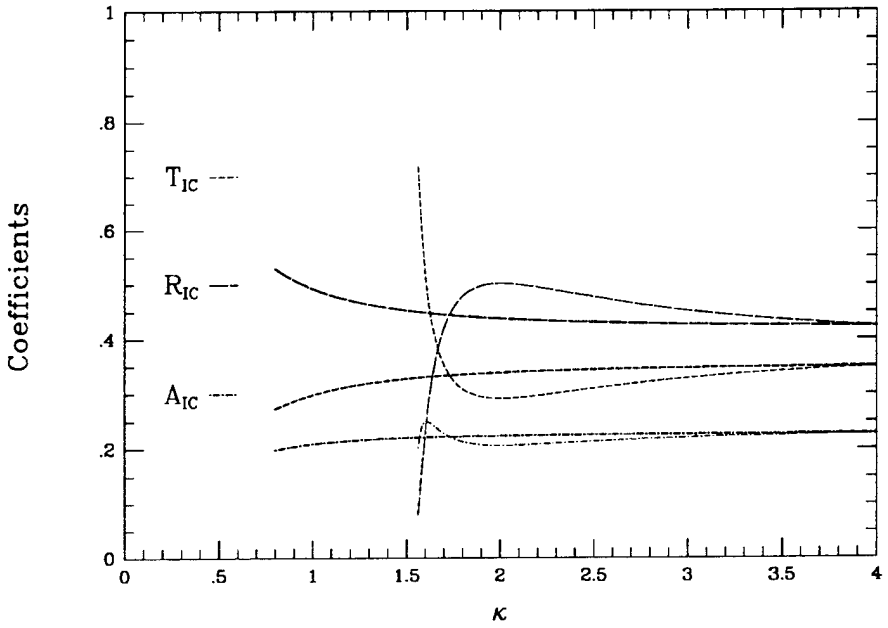

Figure 21: Analytical approximations for the transmission coefficients for $\epsilon = 0.08$ and $\eta = 1\%$ at large κ (which corresponds to large angles of propagation). We have plotted the coefficients related to the phase integral transmission, $\exp(-\pi\beta_+/\epsilon)$, in dark type. The transmission coefficients found from the embedded Budden equation for tunneling through the "gap" are indicated in light type.

tions in a better manner. Rather, it means incorporating more physics into the boundary conditions of the model. For example, we have solved a problem in which the coefficients correspond to transmitted wave flux. However, when these waves reach ionospheric altitudes, they interact with a conducting ionosphere. Wave reflection, transmission, mode coupling and absorption at the magnetosphere-ionosphere boundary are at present a vigorous subject of active research. If, for example, the waves were completely reflected at that boundary, then a transition at a critical κ does not appear because waves are reflected at all κ and, hence, there is no discontinuous jump. If, on the other hand, the transmitted waves are absorbed, then we would expect an abrupt transition at some value of κ which corresponds to reflection at the altitude of the absorbing layer. Moreover, density gradients play a substantial role in determining the exact location of the reflection layer and thus of the exact

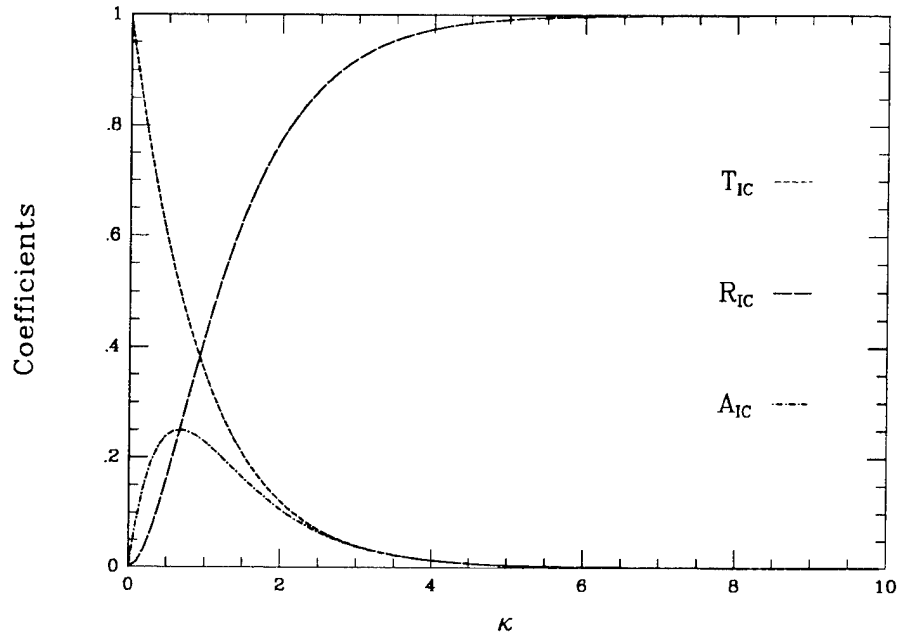

Figure 22: Coefficients for large κ with $\epsilon = 0.08$. Strong absorption is peaked about $\eta = 1$.

behavior of the coefficients with κ.

As an example of the importance of boundary conditions, suppose we were to assume that waves incident on the ionosphere are completely reflected. Then in terms of the phase integral analysis discussed in part 1, we find trivially that for an incident upgoing ion-cyclotron wave from below the ion-gyrofrequency the amount of wave flux $T_{IC} = \exp(-\pi\beta_+/\epsilon)$ continues upward. Because this mode is completely subdominant, it couples to no other modes and hence, the remaining wave power is completely absorbed. Thus, for example, in the case of Figure 12 where no absorption occurs, we would find that 60–70% of the flux transmitted on the coupled branch as C^T_{MS} would be reflected at the ionosphere and then absorbed at the oxygen resonance so that in actuality the coefficients which we have obtained serve as a lower bound.

In sum, our results provide insight with regard to a lower bound estimate of the absorption near the resonance-cutoff-crossover frequency triplet. The results will be somewhat modified if we include more physics into our analysis, but it is certainly clear that substantial wave power is available to heat

minority species ions such as oxygen.

5 Summary

In order to incorporate the presence of coupling both above and below the heavy ion gyrofrequency, check our analytical results, and extract the values of all coefficients, we have solved the system of coupled differential equations (2.1) numerically. In order to integrate the equations around the singularity, we incorporated physical considerations into our analysis. This prescription involved continuing the multivalued solution to the differential equation "above" the pole. By imposing boundary conditions on the numerical solution consistent with downcoming waves in a particular mode, we were able to determine the coefficients associated with wave propagation near the heavy ion gyrofrequency.

We found that our numerical solutions are in reasonable agreement with the analytical solutions that we have obtained. Incident magnetosonic waves couple strongly near the crossover frequency for reasonable values of the minority species density, and for large angle of propagation the waves are completely reflected. Strong absorption (the order of 10–20%) occurs over a substantial portion of the spectrum peaking near perpendicular propagation. Ion-cyclotron waves, on the other hand, undergo Budden-like tunneling at the cutoff frequency for nearly parallel propagation and at the ion-ion hybrid frequency for nearly perpendicular propagation. The absorption is very strong ($\sim$ 20%) over most angles of propagation for reasonable values of the minority species concentration. In either case the absorption levels are consistent with the power required to heat ion conics.

6 Appendix A: Details of Numerical Calculation

In the asymptotic region where the WKB approximation is valid, the solutions to Eq. (2.1) are close to the set of basis functions

$$\begin{aligned}
\Theta_1 &= n_+^{-1/2} \exp\left(-\frac{i}{\epsilon}\int^z n_+(z)dz\right) \\
\Theta_2 &= n_+^{-1/2} \exp\left(+\frac{i}{\epsilon}\int^z n_+(z)dz\right) \\
\Theta_3 &= n_-^{-1/2} \exp\left(-\frac{i}{\epsilon}\int^z n_-(z)dz\right) \\
\Theta_4 &= n_-^{-1/2} \exp\left(+\frac{i}{\epsilon}\int^z n_-(z)dz\right)
\end{aligned} \tag{2.A1}$$

which are asymptotically equivalent to the WKB solutions. The functions $n_\pm$ are solutions to the dispersion relations associated with Eq. (2.1)

$${n_\pm}^2 = \frac{r+l}{2} - \frac{\kappa^2}{2} \pm \left(\left(\frac{r-l}{2}\right)^2 + \frac{\kappa^4}{4}\right)^{1/2} \tag{2.A2}$$

and have nontrivial spatial dependence according to the function, g. For parallel propagation these WKB solutions correspond to a downgoing LHCP wave, upgoing LHCP wave, downgoing RHCP wave, and an upgoing RHCP wave respectively. Indeed, these functions are equivalent to the simpler functions Θ_+^+, Θ_+^-, Θ_-^+ and Θ_-^- respectively of part 1. This set of WKB solutions provides a suitable set of basis functions in the asymptotic regime far away from the pole in the complex plane.

The Poynting flux (2.10) in terms of the upper and lower components, ψ and ϕ, of (2.1) is

$$\mathcal{J} = i(\psi\psi^{*\prime} + \phi\phi^{*\prime} - \psi^*\psi' - \phi^*\phi') \tag{2.A3}$$

In the region where the WKB solutions adequately describe the actual solutions, we find that the coefficients of the WKB solutions ϕ and ψ are algebraicly related by Eq. (2.1). Then to first order in the WKB parameter the Poynting flux above is proportional to

$$\mathcal{J}^+ = -|\gamma_1^+ f_+^+|^2 + |\gamma_2^+ f_+^+|^2 - |\gamma_3^+ f_-^+|^2 + |\gamma_4^+ f_-^+|^2 \tag{2.A4}$$

and the Poynting flux below is analogously

$$\mathcal{J}^- = -|\gamma_1^- f_+^-|^2 + |\gamma_2^- f_+^-|^2 - |\gamma_3^- f_-^-|^2 + |\gamma_4^- f_-^-|^2 \tag{2.A5}$$

where the factors f describe the relationship between the WKB representations of ψ and ϕ. That is

$$f_\pm^j = 1 + \left(\frac{2}{\kappa^2}(n_\pm^2 - r + \kappa^2/2)\right)^2 \tag{2.A6}$$

and the superscript j refers to the location at which this expression is to be evaluated, namely in the asymptotic region where the $\mu^\pm$ have been determined.

The power flow can be identified from the various terms in Eq. (2.A4, 2.A5) so that for the case of magnetosonic incidence as in Eq. (2.11) the coefficients are

$$\begin{aligned} T_{MS} &\equiv |c_3 f_-^-/f_-^+|^2 \\ R_{MS} &\equiv |c_4|^2 \\ C_{MS}^T &\equiv |c_1 f_+^-/f_-^+|^2 \\ C_{MS}^R &\equiv |c_2 f_+^+/f_-^+|^2 \end{aligned} \tag{2.A7}$$

For a downcoming ion-cyclotron wave as in Eq. (2.12) we find

$$\begin{aligned} T_{IC} &\equiv |c_1' f_+^-/f_+^+|^2 \\ R_{IC} &\equiv |c_2'|^2 \\ C_{IC}^T &\equiv |c_3' f_-^-/f_+^+|^2 \\ C_{IC}^R &\equiv |c_4' f_-^+/f_+^+|^2 \end{aligned} \tag{2.A8}$$

Acknowledgements

This work was supported at Massachusetts Institute of Technology by grants from the Geophysics Directorate/Phillips Laboratory (F19628-91-K-0043), Air Force Office of Scientific Research, and NASA, and at the Geophysical Institute by the National Science Foundation contract ATM-91-11509 and the NASA contract NAG 5-1504.

References

Abramowitz, M., and I. A. Stegun, *Handbook of Mathematical Functions with Formulas, Graphs, and Tables.* Dover Publications, Inc., New York, Sec. 9, 13, 1964.

Bender, C. M., and S. A. Orszag, *Advanced Mathematical Methods for Scientists and Engineer.* McGraw-Hill, New York, 1978.

Buchsbaum, S. J., Resonance in a plasma with two ion species, *Phys. Fluids*, *3*, 418, 1960a.

Buchsbaum, S. J., Resonance in a plasma with two ion species, *Phys. Rev. Lett.*, *5*, 495, 1960b.

Budden, K. G., *The Propagation of Radio Waves.* Cambridge University Press, Cambridge, Sec. 19.5, 19.6, 1985.

Chang, T., G. B. Crew, N. Hershkowitz, J. R. Jasperse, J. M. Retterer, and J. D. Winningham, Transverse acceleration of oxygen ions by electromagnetic ion cyclotron resonance with broad band left-hand polarized waves, *Geophys. Res. Lett.*, *13*, 636–639, 1986.

Crew, G. B., and T. Chang, Path-integral formulation of ion conic heating, *Phys. Fluids*, *31*, 3425–3439, 1988.

Crew, G. B., T. Chang, J. M. Retterer, W. K. Peterson, D. A. Gurnett, and R. L. Huff, Ion cyclotron resonance heated conics: Theory and observations, *J. Geophys. Res.*, *94*, 3959, 1990.

Försterling, K., Über die ausbreitung elecktromagnetischer wellen in einem magnetisierten medium bei senkrachter incidenz, *Hochfreq. Elek.*, *59*, 10–22, 1942.

Fuchs, V., K. Ko, and A. Bers, Theory of mode-conversion in weakly inhomogeneous plasma, *Phys. Fluids*, *24*, 1251–1261, 1981.

Fuchs, V., A. Bers, and L. Harten, On the theory of pairwise coupling embedded in more general local dispersion relations, *Phys. Fluids*, *28*, 177–189, 1985.

Gurnett, D. A., S. D. Shawhan, N. M. Brice, and R. L. Smith, Ion cyclotron whistlers, *J. Geophys. Res.*, *70*, 1665–1688, 1965.

Gurnett, D. A., R. L. Huff, J. D. Menietti, J. L. Burch, J. D. Winningham, and S. D. Shawhan, Correlated low-frequency electric and magnetic noise along the auroral field lines, *J. Geophys. Res.*, *89*, 8971–8985, 1984.

Heading, J., The Stokes phenomenon and certain nth-order differential equations ii. The Stokes phenomenon, *Proc. Cambridge Phil. Soc.*, *53*, 419–441, 1957.

Heading, J., *An Introduction to Phase Integral Methods.* Wiley, Methuen, 1962.

Jacquinot, J., B. D. McVey, and J. E. Scharer, Mode conversion of the fast magnetosonic wave in a deuterium-hydrogen tokomak plasma, *Phys. Rev. Lett.*, *39*, 88–91, 1977.

Johnson, J. R., Excitation of low frequency turbulence along auroral field lines, Ph.D. thesis, Massachusetts Institute of Technology, 1992.

Johnson, J. R., T. Chang, G. B. Crew, and M. André, ULF wave propagation along closed field lines in the presence of parallel magnetic field gradients and density fluctuations, *Geophys. Res. Lett.*, *16*, 1469–1472, 1989.

Lashmore-Davies, C. N., V. Fuchs, and R. A. Cairns, Ion-cyclotron resonance heating by means of the fast wave in a longitudinally inhomogeneous magnetic field, *Phys. Fluids*, *28*, 1791–1799, 1985.

Le Quéau, D., and A. Roux, Heating of oxygen ions by resonant absorption of Alfvén waves in a multicomponent plasma, *J. Geophys. Res.*, *98*, 14,929–14,946, 1992.

Lysak, R. L., Auroral electrodynamics with current and voltage generators, *J. Geophys. Res.*, *90*, 4178–4190, 1985.

Lysak, R. L., and C. T. Dum, Dynamics of magnetosphere-ionosphere coupling including turbulent transport, *J. Geophys. Res.*, *88*, 365–380, 1983.

Moore, T. E., D. L. Gallagher, and J. L. H. adn R. H. Comfort, MHD wave breaking in the outer plasmasphere, *Geophys. Res. Lett.*, *14*, 1007–1010, 1987.

Perkins, F. W., Heating tokamaks via the ion-cyclotron and ion-ion hybrid resonances, *Nucl. Fusion*, *17*, 1197–1224, 1977.

Press, W. H., B. P. Flannery, S. A. Teukolsky, and W. T. Vetterling, *Numerical Recipes*. Cambridge University Press, Cambridge, Ch. 15, 1986.

Retterer, J. M., T. Chang, G. B. Crew, J. R. Jasperse, and J. D. Winningham, Monte Carlo modeling of ionospheric oxygen acceleration by cyclotron resonance with broadband electromagnetic turbulence, *Phys. Rev. Lett.*, *59*, 148–151, 1987.

Smith, J., and J. C. Whitson, A numerial study of the system of differential equations for the drift wave in tokomaks, Oak Ridge National Laboratory Report No. CSD/TM-50, Oak Ridge, TN, 1978.

Smith, R. L., and N. M. Brice, Propagation in multi-component plasmas, *J. Geophys. Res.*, *69*, 5029–5040, 1964.

Stix, T. H., *The Theory of Plasma Waves*. McGraw-Hill, New York, Sec. 2.5, 3.5, 1962.

Swanson, D. G., Mode conversion and tunneling at the two-ion hybrid resonance, *Phys. Rev. Lett.*, *36*, 316–319, 1976.

Swanson, D. G., *Plasma Waves*. Academic Press, San Diego, Ch. 6, 1989.